Structural and Magnetic studies of Orthoferrite $BaFeO_{3-\delta}$

A thesis submitted towards partial fulfillment of the BS-MS Dual Degree Program

by

Pravu Prasad Dhal

under the guidance of

Dr. Surjeet Singh

Indian Institute of Science Education and Research (IISER), Pune

Certificate

This is to certify that this thesis entitled "Structural and magnetic studies of Orthoferrite $BaFeO_{3-\delta}$" submitted towards the partial fulfilment of the BS-MS dual degree programme at the Indian Institute of Science Education and Research Pune represents original research carried out by " Pravu prasad dhal " at "INDIAN INSTITUTE OF SCIENCE EDUCATION AND RESEARCH, PUNE", under the supervision of "Dr.Surjeet Singh" during the academic year 2013-2014.

Student
Name

Supervisor
Name

Acknowledgements

- I would like to express my gratitude to my supervisor Dr. Surjeet Singh for providing me the opportunity to work on this project and for his active encouragement as well as for his consistent guidance. I am indebted to him for having helped me shape the problem and providing insights towards the solution.
- I sincerely thank IISER, Pune for providing me this wonderful platform to do extensive research.
- I would like to especially thank all my labmates Koushik Karmakar, Rabindranath Bag, Prachee Telang, Vinayak Kulkarni, Rohit Kumar for their selfless support and for the useful discussions.
- I thank Anil Shetty for his help in carrying out the SEM measurements.
- I would like to thank Neelesh Dumbre and Prashant Kale for their immense help in setting up our instruments.
- I must thank all my friends for their extensive support and encouragement during my MS life at IISER Pune.
- At last, but not the least, I sincerely express my gratitude to my family who have been acting as a pillar of great strength through every single moment of life.

DEDICATED TO '09 BATCH OF IISER, PUNE

Abstract

The orthoferrites $BaFeO_{3-\delta}$ can adopt several competing structural phases depending on the oxygen content $(3-\delta)$ of the formula unit which can be varied continuously between $\delta = 0$ to $\delta = ½$. The end members at $\delta = 0$ and $\delta = ½$ correspond, respectively, to structures with cubic and monoclinic symmetries. The $\delta = ½$ member having the monoclinic symmetry has the well-known Brownmillerite type structure. For intermediate values of δ, structures with hexagonal, tetragonal, rhombohedral and cubic symmetries have been controversially reported by several authors. In this thesis, we investigated the conditions required for the formation of these various phases and those for growing single-crystal of the Brownmillerite phase $Ba_2Fe_2O_5$ ($\delta = ½$). Effect of La doping on the structural and physical properties of $BaFeO_{3-\delta}$ were also studied. The polycrystalline samples of $BaFeO_{3-\delta}$ and their La-doped variants were obtained by using the conventional solid-state reaction route under varying heat-treatment conditions. The single-crystal of the Brownmillerite phase is grown using the floating-zone method associated with a four-mirror image furnace. We find that $BaFeO_{3-\delta}$ synthesized under air in the temperature range 1183-1373 K and with a cooling rate of 450 K/h crystallizes with a hexagonal structure. The same samples when annealed at 1373 K under flowing oxygen tended to be impure containing small quantities of unidentifiable impurities. Attempts to synthesize the tetragonal phase under different sintering conditions always resulted in a multiphase sample consisting of a mixtures of hexagonal and monoclinic phases. The Brownmillerite phase, on the other hand, could only be synthesized at temperatures above 1473 K in air with subsequent quenching. Using this as the primary information, attempts were made to grow single crystals of the Brownmillerite phase using a rapid growth technique in an image furnace. Preliminary work suggests that the floating-zone can be stabilized under synthetic air with growth speeds ranging from 5 to 10 mm/h. La-doping in the hexagonal $BaFeO_{3-\delta}$ tends to stabilize the tetragonal phase. While 1 % La-doped sample retains the hexagonal structure, the sample with higher La-doping contained increasing amounts of the tetragonal phase. The sample with 20 % La-doping is found to be purely tetragonal. Magnetization measurements were performed on pure $BaFeO_{3-\delta}$ (hexagonal) and 20 % La-doped $BaFeO_{3-\delta}$ (tetragonal) samples. Both samples show weak ferromagnetism at low temperatures as inferred from hysteresis loops in their isothermal magnetization measured at T = 2 K. The temperature variation of magnetization of the undoped sample exhibits magnetic anomalies near T = 250 K, 170 K and 110 K. In the La doped sample corresponding anomalies were present, however, they appear at lower temperatures of T = 225 K, 70 K and 40 K, respectively. The possible origins of this magnetic anomalies is discussed. The resistivity measurements show an increase of the electrical conductivity due to the electron-doping in the La-doped samples.

Contents

Chapter 1

Introduction

Pervoskites have the chemical formula ABO_3 where A is typically an alkaline or rare-earth metal ion and B is a transition metal ion. The ideal structure consists of A ions located at the vertices of a cubic unit cell whose body-center and face-centers are occupied by B and O ions, respectively. Perovskite structure allows a huge degree of flexibility in terms of the choices of A and B elements and also to the degree of oxygen content per formula unit. Materials derived from perovskite structure often exhibit interesting physical and chemical properties and have found applications in several cutting edge technologies [1-5]. Some prototypical examples of perovskite based materials include $BaTiO_3$ which is ferroelectric at room-temperature (T_C = 400 K) [29], another closely related perovskite compound is $SrTiO_3$ which shows very interesting quantum paraelectric behavior with very large dielectric constant [37], in $YTiO_3$ the orbital ordering of the Ti 3d orbitals represents a novel magnetic ground state [30] and in $LaMnO_3$, a metal-insulator transition and associated colossal magneto resistance upon hole doping is of significant fundamental interest and has found applications in data storage devices. In recent 'green' energy initiatives perovskite materials are playing an important role. For example, some of the perovskites have been shown to be useful materials for Solid Oxide Fuel Cells (SOFCs) and thermoelectric devices owing to their structural stability under oxidizing atmospheres and high temperatures, and also because of their low production cost.[3, 5-9 10, 11 1, 12,38] . $La_{0.8}Sr_{0.2}MnO_{3-\delta}$, for instance, has been used as a conventional oxygen reduction electrode in high temperature SOFCs due to high ionic conductivity [5, 12]. Pervoskite-type materials have also been used as electrochemical gas sensors for the detection of oxidizing gases, such as, oxygen, ozone etc [3]. For example, $LaCu_{0.3}Fe_{0.7}O_{3-\delta}$, $La_{0.05}Sr_{0.95}Ti_{0.65}Fe_{0.35}O_{3-\delta}$ have been studied as O_2 sensors which show low temperature dependency and fast response time [13]. Recently, a class of iron containing perovskites $AFeO_3$ (where A can be alkaline or rare-earth metal ion) have attracted considerable attention due to their possible multiferroic behavior (mutually coexisting ferroic orders) [39]. In particular, alkaline metal based orthoferrite containing Fe in its high-oxidation state (Fe^{4+}) are of considerable importance. The oxides containing Fe^{4+} generally behave differently from those containing Fe^{3+} and Fe^{2+}. For example, FeO and $LaFeO_3$ are antiferromagnetic insulators and Fe_3O_4 is ferrimagnetic with an insulating gap of 0.11 eV. On the other hand, Fe^{4+} containing oxides tend to show a shift towards ferromagnetism and metallicity. $SrFeO_3$ for instance is weakly ferromagnetic below about T = 140 K but becomes a genuine ferromagnet under external pressure. The present thesis focuses on more specific orthoferrites $BaFeO_{3-\delta}$. $BaFeO_{3-\delta}$ is known to exist with varying crystal structures over a wide range of oxygen contents $(3-\delta)$. The fully oxygenated sample (x = 0)

having the cubic perovskite symmetry cannot be easily stabilized. Very recently, Hayashi et al. [22], used ozone as an oxidant to obtain this compound as a single cubic phase. $BaFeO_3$ is unique in several ways. Firstly, it is one of those rare compounds with iron in its high oxidation state (Fe^{4+}: d^4), secondly, the Fe^{4+} spins order ferromagnetically below T = 100 K and the Curie-temperature is reported to exceed room-temperature under pressures as high as 400 GPa. The other end member with the Brownmillerite structure (x = 0.5) can be prepared under air atmosphere at high temperature sintering and subsequent quenching. The Brownmillerite (BM) phase has the stoichiometry $Ba_2Fe_2O_5$ with iron in its usual 3+ (d^5) oxidation state. The study of the BM phase could be of great relevance because its structural unit contains alternating layers of octahedrally and tetrahedral coordinated Fe^{3+} ions and these are proposed to be potential multiferroic materials [39]. As far as the intermediate values of δ are concerned, there has been controversial reports of structural phases with hexagonal, tetragonal, rhombohedral and triclinic symmetries [18,19,23]. Moreover, there is no comprehensive report of the magnetic and multiferroic properties of these compounds. Under this project work we investigated the conditions required for the formation of these various phases and those for growing single-crystal of the Brownmillerite phase $Ba_2Fe_2O_5$ (x = 0.5). Effect of La doping on the structural and magnetic properties of $BaFeO_{3-\delta}$ were also studied.

1.1 Crystal Structure

1.1.1 Basic Perovskite structure

Compounds having ABO_3 perovskite-type structure can be considered as the basic structure from which compounds with other structure types can be derived. In the ideal cubic unit cell of such a compound, cation A is situated at the corner of the cube (0, 0, 0), cation B sits at body centered position (1/2, 1/2, 1/2) and the O^{2-} ions are situated at the face centered positions (1/2, 1/2, 0). The B-cation in the ideal cubic-symmetry is in 6-fold coordination which is surrounded by an octahedron of anions, whereas the 'A' cation is in 12-fold coordination. The 'A' atom is normally bigger than the 'B' atom.

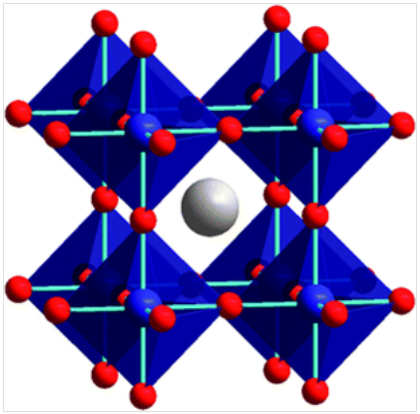

Figure 1.1: Perovskite ABO_3 structure in its Cubic form [46]. The Grey ball at the centre represents A ion, the blue balls are the B ions and the red balls are the oxygen ions.

The relative ion size requirements for stability of cubic structure is quite stringent. Slight distortion in the structure can change the coordination numbers of both 'A' and

'B' cations. Tilting of BO_6 octahedra can reduce the coordination of 'A' cation from 12 to 8. Several combinations are possible for the choice of 'A' and 'B' cations. Generally 'A' is alkaline or rare-earth metal (e.g., La, Ba, Sr, Ca etc.) and 'B' is a transition metal ion (e.g., Ti, Fe, Co, etc.). In general, pervoskites deviate from cubic structure because of different reasons which can be due to i) shifting of the position of 'A' and 'B' cations from their respective sites, ii) deformation of the octahedra iii) elongation of the whole unit cell in one direction making it distorted or due to the rotation of the octahedra.

1.1.2 Effect of cation substitution on structure

In this system, ionic radii of 'A' and 'B' cations are different and govern the internal strains in the compound. The size mismatch is responsible for distinct stacking and rotation of the octahedra resulting in lowering of the symmetry, which can be as low as triclinic. The Goldschmidt tolerance factor(t) is generally used to quantify the internal strain and is given in terms of ionic radii or as a function of inter-atomic bond lengths [14].

Goldschmidt tolerance factor is given as

$$t = \frac{r_a + r_o}{(r_b + r_o) * \sqrt{2}} \text{ or } t = \frac{d_{Ao}}{d_{Bo} * \sqrt{2}}$$

where

r_A = Atomic radii of 'A' cation.

r_O = Atomic radii of oxygen ion.

r_B = Atomic radii of 'B' cation.

d_{AO} = Bond length between A and O.

d_{BO} = Bond length between B and O.

The strain is minimal for t = 1 which corresponds to the ideal cubic perovskite structure. In practice, the cubic symmetry remains for $0.9 < t < 1$. But if t lies outside this interval, the BO_6 octahedra undergoes rotation or distortion to compensate for the non-ideal ionic sizes resulting in lowering of the symmetry altering the unit cell to form superstructures. For instance, for $t > 1$, A – O bond distance increases and the structure becomes rhombohedral (example: $BaTiO_3$ for which t = 1.06 [29]). On the other hand, the structure is compressed and becomes tetragonal (or Orthorhombic) for $t < 1$. $GdFeO_3$ is a classic example of this case where the A-site cation is not large enough for the space between the octahedra resulting in tilting of octahdra and giving rise to an enlarged orthorhombic Pbnm unit cell [40].

1.2 Variation of ABO_3 stoichiometry

1.2.1 Possible derivatives

Perovskite ABO_3 can be thought of as the parent structure from which related structures can be derived [46]. For instance, one can derive the pyrochlore ($A_2B_2O_7$) type structure through oxidation and Brownmillerite ($A_2B_2O_5$) type structure through reduction of the ABO_3 phase.

1.2.2 Intermediate phases

Compounds with various oxygen-deficient phases can be obtained by reducing perovskite phase using different techniques such as giving different thermal treatment, controlling partial pressure of different oxidizing and reducing gases. $ABO_{3-\delta}$ system may exhibit different lattice structure for different values of 'δ' due to the ordering of oxygen vacancies. There are several compounds like $SrFeO_{3-\delta}$, $LaFeO_{3-\delta}$, $SrCoO_{3-\delta}$ and $BaFeO_{3-\delta}$ which show this phenomenon. For example, $SrFeO_{3-\delta}$ can be stabilized into four distinct phases for the value of $\delta = 0$, 0.125, 0.25 and 0.5. Similarly, $BaFeO_{3-\delta}$ system acquires different structures for different values of 'δ'. The structures reported include those with cubic, Monoclinic, Rhombohedral, Tetragonal and Hexagonal symmetries [18,19,23]. The removal of O^{2-} anions from $ABO_{3-\delta}$ lattice creates vacancies which changes the coordination number as well as the valence state of the B cations.

1.2.3 Brownmillerite phase

The Brownmillerite phase has the stoichiometry $A_2B_2O_5$. The formation of this phase generally depends on the synthesis technique and on the type of cations involved. Some possible combinations of 'A' and 'B' include: 'A' = Ca, Ba,Sr and 'B'= Al, Fe and Co. Since, the oxygen vacancy is maximum for Brownmillerite phase, hopping of ion from one vacant site to other increases which leads to very large ionic conduction. The crystal has a sandwiched like structure where BO_6 octahedral layers is sandwiched between slabs of BO_4 tetrahedral chains. These tetrahedral chains are separated by one dimensional vacancy chains. Similarly, A2BB'O5 Brownmillerite-type structure can be explained by a sequence of $AO - BO_2 - AO - B'O_\Delta - AO$- layers, where '$\Delta$' symbolizes oxygen vacancy, as shown on figure 1.2.

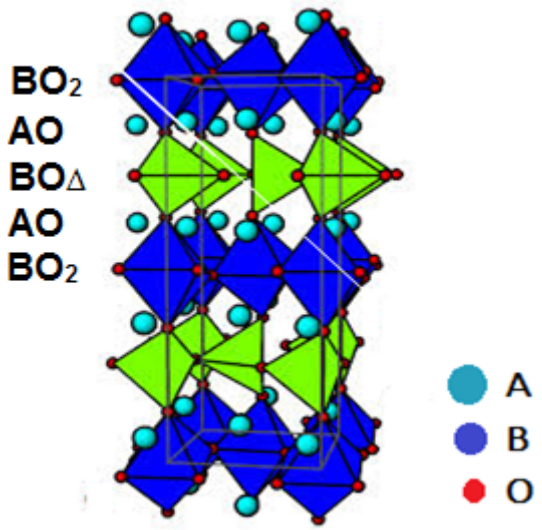

Figure 1.2: Basic Unit cell of Brownmillerite-type structure, space group, Pnma made of layers of octahedra separated by layers of tetrahedral chains. [44]

There are two different sites which are possible for transition metal ions, called B and B', having different coordination number 6 and 4 respectively. 'B' sites refer to octahedra and 'B' ' sites correspond to tetrahedra. The $B'O_4$ tetrahedra are connected by corners

and form 1-D chains lying in the [110] direction of the perovskite cell. In the $B'O_{\Delta}$ layers, due to cooperative rotations of tetrahedra within the chains , both B' and O atoms are shifted from their respective position in the perovskite lattice structure[35].

1.3 Magnetism in Oxides

We shall now briefly review magnetism in transition metal ions. The material presented here is essentially general and can easily be found in several textbooks in magnetism .Iron is one of the transition metal element having a 3d electronic structure. These 3d transition metals especially their oxides are very important in the study of magnetism. This section covers the theory of magnetism, mean field theory, the exchange interactions between magnetic atoms and the crystal field environment they inhabit and at the end the behavior of isolated magnetic moments.

1.3.1 Magnetic moments

The magnetic moment 'μ' of an atom is associated with its total angular momentum 'J' given by:

$$J = L + S,$$

where

L= Orbital angular momentum.
S= Quantum number associated with the intrinsic spin of the electron.

The relationship between the magnetic moment 'μ' and the total angular momentum 'J' is given by the equation

$$\mu = g_J \mu_B \sqrt{J(J+1)}$$

In this equation

μ_B =Bohr magneton, where, $\mu_B = \dfrac{e\hbar}{2m_e} = 4\pi \times 10^{-7} N.A^{-2}$.

g_J =Lande g-factor, which can be expressed in terms of the quantum numbers J, L and S, as follows:

$$g_J = \frac{3}{2} + \frac{S(S+1) - L(L+1)}{2J(J+1)}$$

The magnetic susceptibility 'χ' is a measure of the magnetic response of a material under a small external magnetic field and is defined as:

$$\chi = \frac{M}{H},$$

where,
M = magnetization which is magnetic moment per unit volume.
H =Applied magnetic field.

1.3.2 Paramagnetism

In a paramagnetic state magnetic moments are considered independent (non-interacting) and are in state of constant thermally driven orientational disorder. In the presence of an applied magnetic field (typically of the order of 100 Gauss) the moments tend to align parallel to the applied magnetic field, however, the thermally driven disorder does the opposite (i.e., opposes any kind of alignment); consequently a partial alignment ensues (to be more precise, a small non-zero component of each moment appears along the field direction). Cooling the sample, weakens the thermal effect and the magnetization (i.e., magnetic moment per unit volume in the direction of the applied magnetic field) increases in magnitude. Curie law provides a quantitative description of the variation of magnetization (or magnetic susceptibility) in the paramagnetic state. By applying the Boltzmann statistics, it can be easily shown that the magnetic susceptibility in the paramagnetic state is given by $\chi = \dfrac{C}{T}$ where C is the Curie constant and T is temperature of the sample measured in the units of Kelvin. The Curie constant C is given as

$$C = \frac{N_A \mu^2}{3K} \text{ (CGS unit)}$$

Here, N_A is the Avogadro's number; and μ is given by

$$\mu^2 = \mu_B^2 g_J^2 J(J+1),$$

In most real systems, however, the magnetic interactions (typically between the nearest neighbors) are non-negligible. In such a scenario, the magnetic material undergoes a phase transition near temperatures given roughly by $k_B T_C = J$, where J is the strength of 'exchange' interaction between the neighboring moments and k_B is the Boltzmann constant. Note the use of the word 'exchange' to emphasize the quantum mechanical origin of the magnetic interactions (except when it arises solely due to the dipolar interactions, which are far too weak in most cases to be of any significance). Returning to the main point of discussion, we now have two temperature regions: a region below T_C where the moments are ordered and a region sufficiently above T_C where the moments are in a thermally driven disordered state (as for paramagnet discussed above). In this high temperature range, a modified Curie law (known as Curie-Weiss law) can be derived with the mean field framework. The law states that the susceptibility of an interacting system (nearest neighbor interactions non-zero) in the temperature range above T_C is given by: $\chi = \dfrac{C}{T - \theta_p}$, where C as before is the Curie constant and θ_P is the paramagnetic Curie temperature which coincides with the actual T_C within the mean-field framework.

1.3.3 Diamagnetism

Diamagnetism is a weak effect which gets always induced no matter what the nature of the sample under investigation is. However, being a weak effect, its omnipresence has any significance only when the other forms of magnetization (to be discussed later) are not present. Weak induced magnetic moment of the diamagnetic materials align in the

opposite direction of the applied magnetic field to oppose the external magnetic field. Unlike paramagnets, the diamagnetic response is largely temperature independent and the diamagnetic susceptibility is always negative since the moments are induced in a direction opposite to that of the applied magnetic field.

1.3.4 Ferro-, antiferro- and ferrimagnetism

Permanent magnets that can be magnetized by applying external magnetic field and remain magnetized even if the applied field is removed are either ferromagnetic or ferrimagnetic. Let us first talk about ferromagnets. Their most common examples are Iron, Nickel and Cobalt (note that all three are metals, i.e., ferromagnetism and metallicity usually go together). In a ferromagnet, there is only type of magnetic ion (i.e., moment size at each magnetic lattice point is the same). Below a certain temperature (called the Curie temperature) these moments spontaneously align along a certain spatial direction. In an isotropic ferromagnet (i.e., isotropic moments), all direction are equally favorable, minor or residual fields or interactions present in the system make one of the directions slightly more energetically favorable over the others. However, most ferromagnets are anisotropic (i.e., moments are constrained to point either along a certain direction or are confined to a certain crystallographic plane) in such cases one of the crystallographic directions is preferred over the others. The preferred direction is called the easy-axis. In iron, for example, the easy-axis is along the crystallographic (100) direction and in Nickel the easy-axis is along the (111) direction. This is a fundamental effect called magneto-crystalline anisotropy. Above, we mentioned that below T_C, all the moments align along a certain spatial direction. This would mean that the magnetic field due to all the moments would add up to give rise to a large magnetic field spread over the entire space. Such a thing would cost a large magnetic energy to the system. In order to avoid paying such large energy costs, a ferromagnet typically has domains. Within each domain the moments point along the same crystallographic direction, however, on traversing from one domain to the adjacent domain the orientation switches to another equivalent crystallographic direction (for instance for iron if the magnetization in domain A points along (100), in the neighboring domain they may point along the (010) direction (or any one of the other 5 equivalent directions). The region that separates two adjacent domains is called the domain-wall. If the magnetization switches by 90^o between the two adjacent domains it is called a 90^o domain wall and if does by 180^o (e.g., from (100) to $(\bar{1}00)$ in the above example), it is called a 180^o domain wall. Magnetization measured at a fixed temperature as a function of applied magnetic field is called isothermal magnetization. In a ferromagnet, the isothermal magnetization below the Curie temperature is characterized by the following quantities: saturation magnetization: a state where the magnetization in all the domains point along the direction of the field or in other words the domain with magnetization pointing along the field direction (favorably arranged domain) expands at the expense of those that are arranged unfavorably. Magnitude of the saturated magnetization can be used to calculate the magnetic moment at each magnetic lattice site. Typically, for rare-earths (both oxides and intermetallics) this value matches with the free-ion value (i.e. the value of the magnetic moment for an ion in vacuum taking both L and S into account). The magnetic moment of the transition metal oxide (of at least the iron group) is typically given by the total spin angular momentum, orbital angular momentum being quenched due to the crystalline electric field of the neighbors. In transition metals (Iron group), the magnetism is itinerant and the magnetic moment per atom is

smaller than the calculated value. In itinerant ferromagnets the spontaneous magnetization arises due to splitting of the electron energy band at Fermi level. Antiferromagnets are those where below a certain temperature (called the Néel temperature) the spins on any two neighboring magnetic sites order anti-parallely. The resultant spin structure has an ...-up-down-up-down-... kind of arrangement. One can think of this arrangement as a superposition of two interpenetrating ferromagnetic sublattices such that the ferromagnetic order of one is opposite to that of the other. Antiferromagnets are more common than the ferromagnets. Some examples of magnetic materials showing antiferromagnetic order are: a large number of transition metal oxides, for example, NiO and La_2CuO_4; intermetallic compounds, such as $CeIn_3$, MnNi, etc. Among elements, Cr and Mn order antiferromagnetically, most rare-earth metals also show antiferromagnetically ordered ground state though admittedly the ordered spin structure in most rare-earths is often more complicated than in a simple Néel type antiferromagnet. A ferrimagnet consists of two magnetic sublattices (say, A and B) occupied by two different kinds of magnetic ions. The classic example of ferrimagnets is the compound based on Spinel (or inverse spinel) A_2BO_4 structure. For example, Fe_3O_4 or $Fe^{3+}(Fe^{2+}Fe^{3+})O_4$ where Fe^{3+} at the A site couples antiferromagnetically to the Fe^{2+} and Fe^{3+} at the B site of the inverse spinel structure resulting in a ferromagnetic structure. Interestingly, under small applied magnetic fields the net magnetization of a highly anisotropic ferrimagnet can become negative below the so-called compensation temperature.

1.3.5 Crystal field splitting

Crystal field theory generally describes the breaking of orbital degeneracy of d or f orbital due to the static electric field created by surrounding charge distributions of the anions or the ligand ions. Five degenerate d orbitals, which are d_{xy}, d_{yz}, d_{xz}, $d_{x^2-y^2}$, d_{z^2}, can be grouped as three t_{2g} (d_{xy}, d_{yz}, d_{xz}) and two e_g $(d_{x^2-y^2}, d_{z^2})$ orbitals. The electrostatic repulsion between the electrons of ligand ions and the d orbitals results in a partial lifting of the degeneracy to d orbitals. In an octahedral complex, the d orbital splits into two sets of energy level where t_{2g} orbitals having lower energy then the e_g orbitals. In the tetrahedral symmetry, the reverse occurs with t_{2g} having higher energy and the e_g orbitals which can easily be understood by considering the spatial orientations of these orbitals with respect to the Ligand ions.

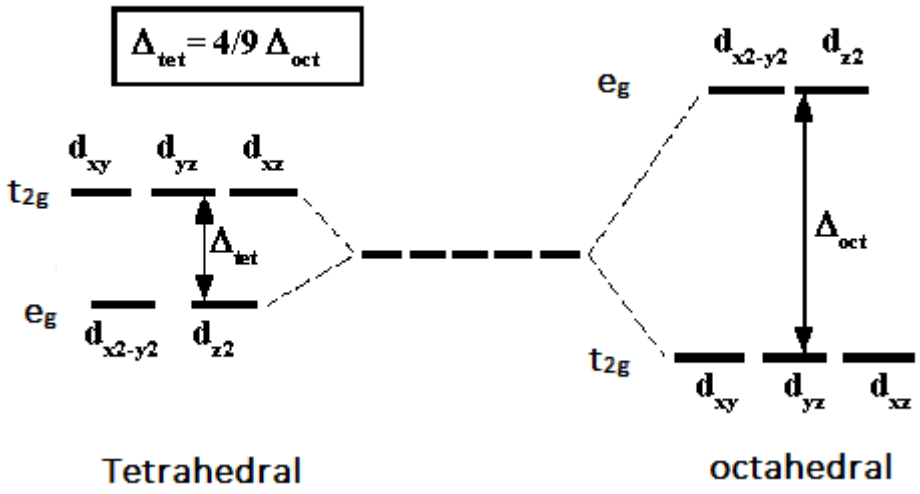

Figure 1.3: Shows the crystal field splitting of 'd' orbitals of Tetrahedral and Octahedral complexes.[41]

Normally, Iron has d^6 electronic configuration and can exist in several oxidation states such as Fe^{2+}, Fe^{3+} and Fe^{4+}. The electronic configurations of these states are d^6, d^5, and d^4 respectively. The most common configurations are $Fe^{2+}$and Fe^{3+}. Very few compounds having iron in Fe^{4+} oxidation state are known or reported. Electrons are filled in the energy levels according to the Hund's rule. When the crystal field energy is higher than the pairing energy, then pairing occurs at the lower energy states before filling the higher energy states. This makes the total spin less and therefore called as the 'low spin' state. Other case is the 'high spin' case where all the energy levels are filled first before the pairing occurs.

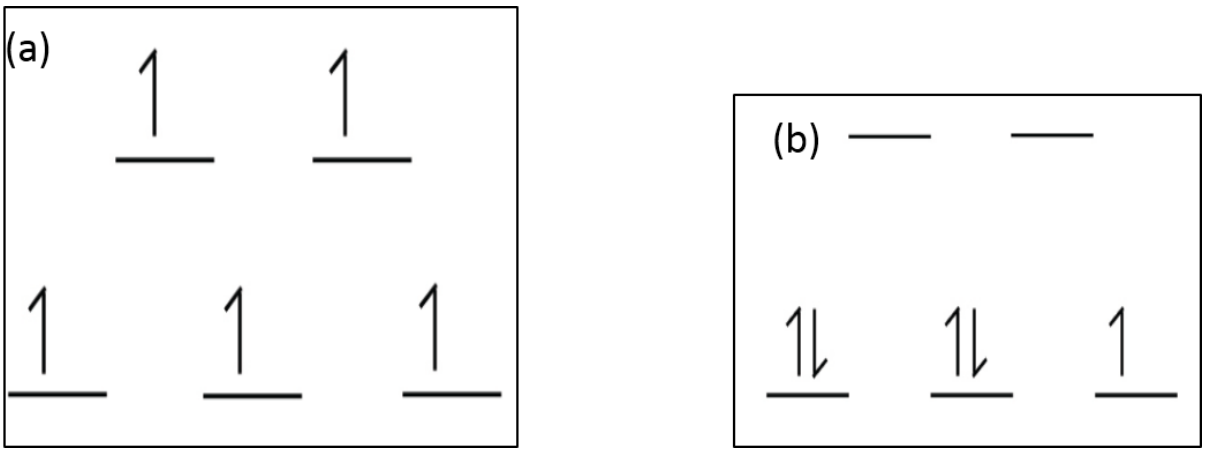

Figure 1.4: Illustrate the high spin and low spin case respectively.

1.3.6 Exchange interactions

Materials containing magnetic ions often show long-range ordering of the magnetic

moments (we discussed above the case of ferro- antiferro- and ferromagnetic order of the moments) because of exchange. For the exchange interaction to be direct, the orbitals of neighboring ions should overlap which normally occurs in the case of transition metals such as Iron. However, in transition metal oxides, often the neighboring magnetic ions have an intervening anion which couples their magnetic moment indirectly. Such an indirect exchange is called super exchange and it is represented schematically in figure below in the case of $Mn^{3+}-O-Mn^{3+}$ (as in $LaMnO_3$).

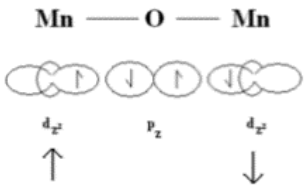

Figure 1.5: Shows schematic representation of superexchange[42]

Ferromagnetic ordering and associated conductivity arise due to the phenomenon of double exchange as for example in $La_{1-x}Sr_xMnO_3$ (i.e., hole doped Mott insulator) where the e_g electron can hop from one Mn^{3+} to a neighboring Mn^{4+} via the intervening oxygen. Since hopping can only occur between ferromagnetically aligned spin, therefore ferromagnetic alignment is favorable.

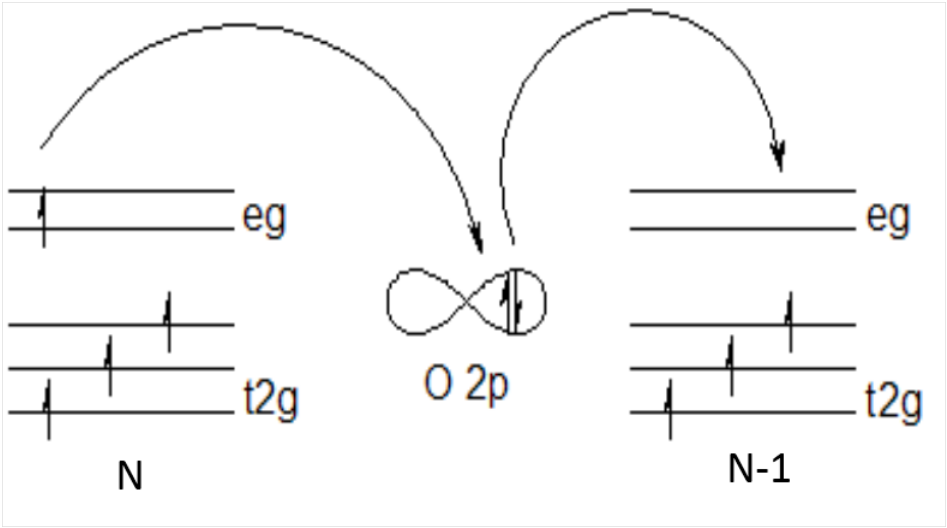

Figure 1.6: Illustrates the double exchange in mixed valence state through oxygen atom. (Source: Wikipedia)

1.3.7 Spin State Transitions

In section 1.3.5 , we discussed that electrons in iron atoms can exist in different spin states depending on the crystal field environment. This spin state transitions are not generally favorable in perovskites containing manganese and copper ions, but they are possible in materials containing iron and cobalt ions[19]. All the three possible spin states of iron are illustrated in figure 1.9.

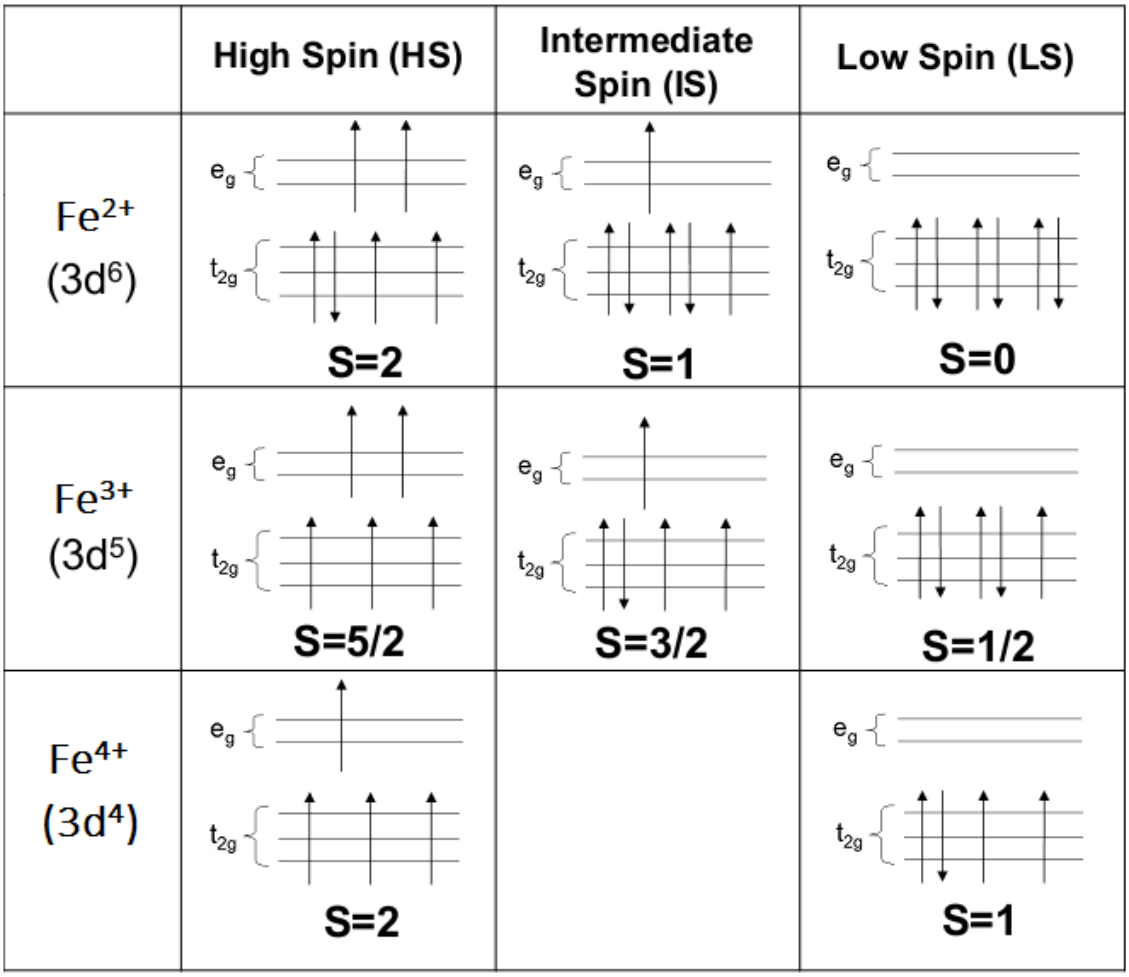

Figure 1.7: The electronic configuration of Fe^{2+}, $Fe^{3+}$and Fe^{4+} in an octahedral environment in high spin, intermediate spin and low spin cases.

Chapter 2

Experimental Techniques

This chapter includes all the experimental techniques that were used for the sample preparation, their structural characterizations and for measurement of various physical properties. These techniques are discussed in sections 2.1, 2.2, 2.3, respectively. Briefly, the samples were prepared using the conventional solid state reaction route under various sintering conditions. Structural characterizations of the synthesized samples were done by using scanning electron microscopy equipped with energy dispersive x-ray analysis tool and powder X-ray diffraction. Single-crystals were grown using a 4-mirror image furnace. The magnetic properties of the samples were studied by using Physical Properties Measurement System (PPMS) and resistivity measurements were done on a home-built set-up using a Four-Probe method.

2.1 Sample Preparation

Samples were prepared using the conventional solid state reaction route. The starting precursors ($BaCO_3$ and Fe_2O_3) were high purity reagents. They were weighed as per the stoichiometry and mixed thoroughly in a mortar and pestle for about 45 min and placed in an alumina crucible for the solid-state reaction at high temperatures. The process of solid-state reaction involves slow diffusion and reaction of the molecules of the two species to form the desired compound. The solid-state reaction is more effective when the reaction product is subject to intermediate grindings and often pelletizing the reaction product accelerates the reaction process. In the present work, we always calcined the sample first before pelletizing it. The pellets were made by casting in the samples in a 12 mm diameter stainless steel die using uniaxial pressures up to 10 bar. The heat-treatments were carried out using the muffle and tube type furnaces. In the tube furnace, water cooled vacuum flanges were used to ensure high purity of the sintering atmosphere which is crucial in the present case because of the sensitivity of $BaFeO_{3-\delta}$ to the oxygen partial pressure in the reaction medium. The temperature was controlled using a Eurotherm (model 3504) temperature controller.

2.1.1 Single crystal growth of $Ba_2Fe_2O_5$

The single crystal of $Ba_2Fe_2O_5$ was grown by using a four-mirror optical floating zone furnace (from Crystal system Corporation, Japan). A schematic diagram of the vertical section of an optical floating zone furnace is given in figure 2.1. The image furnace consists of four halogen lamps, each placed at the focus of a semi-ellipsoidal shape reflector. The

second focus of each reflector coincides at a certain point on the vertical axis of the furnace inside the growth chamber. The growth chamber is enclosed by using a quartz enclosure which not only allows the light flux to travel unhindered but also help in maintaing the growth atmosphere. After the reflection from the walls of the reflectors, the energy flux of all the lamps converge at the second foci, where a molten zone is formed between the polycrystalline feed and the seed rod. The feed rod is normally suspended from the upper shaft of the furnace using nickel wire while the seed rod is clamped to the lower shaft by using an alumina holder.

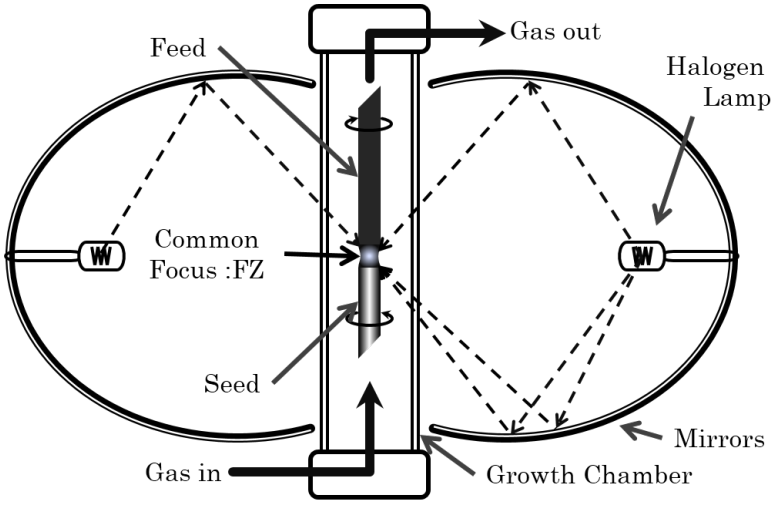

Figure 2.1: Schematic diagram of the vertical section of the optical furnace[36]

2.2 Characterization

2.2.1 Powder X-ray Diffraction

Powder X-ray diffraction is a preferred method of identifying the crystal structure symmetry of a compound. Often, if the compound being synthesized is already known to exist one can find its calculated or experimental X-ray diffraction pattern in a large database compiled by Joint Committee on Powder Diffraction Standards (JCPDS). Powder diffraction provides a rapid and non-destructive analysis of multi component mixtures. This method is widely used to identify and characterize crystalline solids, which produce a distinctive diffraction pattern. The position of peaks corresponding to lattice spacing and their relative intensities are indicative of a particular phase of a material. A multiphase sample shows more than one pattern superposed while single phase shows distinct peaks. In the the present work, X-ray of all the samples were collected using Bruker D8 Advance powder X-ray diffractometer. As illustrated in figure 2.2, it consists a monochromatic source of X-rays, usually from a copper target or anode giving the characteristic CuKα radiations (λ=0.154 nm after passing through nickel filter), sample holder and X-ray detector. X-ray data was collected by performing a scan on 2ϑ range of $10 - 80^0$ with an angular step of 0.01^0 and using a scan speed of 0.5 sec/step. Then XRD patterns of all the samples were compared with the standard data base.

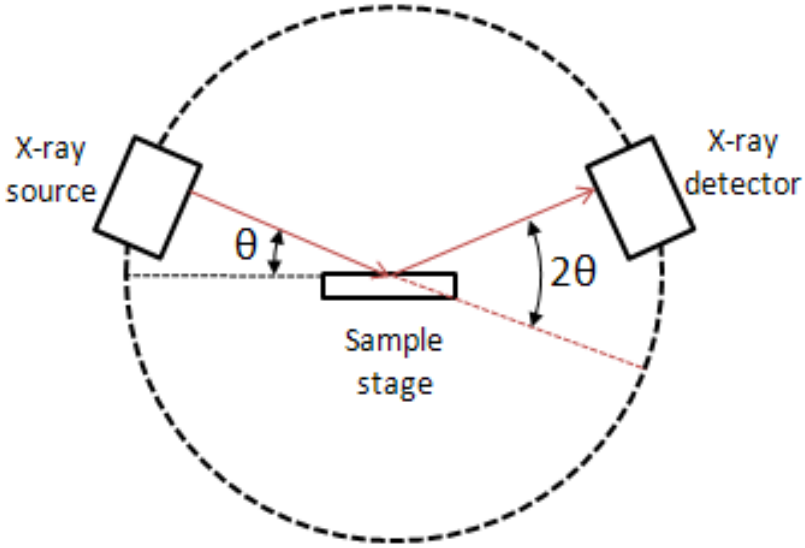

Figure 2.2: Schematic diagram of X-ray Diffractometer [45]

2.2.2 Scanning Electron Microscope technique

FE-SEM technique is generally used to study the sample's surface morphology and composition. This is one type of electron microscope which produces images of the sample by scanning it with a focused beam of electrons. The electron beam is generated by heating a Zirconium oxide coated Tungsten filament. SEM can achieve resolution more than 1nm and can be operated at energies in between 0.1 KeV to 30 KeV. Specimens can be observed in high vacuum as well as in wet conditions. We did SEM analysis of our samples in presence of high vacuum of the order of 10^{-6} bar. Scanning electron microscope uses angular back scattered electrons from the sample for imaging. In an electron microscope, the electron beam can be focused to a very small spot size using electrostatic or magnetic lenses, but usually electrostatic lenses are used for an SEM. The fine beam is scanned on the sample surface using a scan generator and back scattered electrons are collected by a detector. This also can be used to obtain the composition of the sample by using a technique known as Energy Dispersive Analysis of X-rays (EDAX). The high energy electrons interact with the sample and produce characteristic X-rays of the constituent atoms. The composition can be obtained by comparing the intensities with the given database.

2.2.3 Physical Properties Measurement System

Physical Properties Measurement System (PPMS) can be used to measure different physical properties of samples such as electrical properties, magnetic properties, thermal transport properties, etc. Sample environment controls include magnetic fields up to $\pm$ 9 Tesla (using a superconducting magnet) and temperature range of 2.0 to 400 K. 'DC'- susceptibility measurements were done using VSM (Vibrating sample Magnetometer), which is a part of PPMS. This operates on Faraday's Law of Induction, which tells us that a

changing magnetic field will produce an electric field. A VSM operates by first placing the sample in a constant magnetic field. If the sample is magnetic, this constant magnetic field will magnetize it by aligning the magnetic domains, or the individual magnetic spins, with the field. The magnetic dipole moment of the sample will create a magnetic field around the sample. As the sample is moved up and down, this magnetic field changes as a function of time and can be sensed by a set of pick-up coils. In our experiments, we used powder samples filled in a 'non-magnetic' polymeric capsule. The typical sample mass was around 40 mg and the sample was vibrated at a fixed frequency of 40 Hz and an amplitude of 2 mm.

2.2.4 Four Probe Resistivity Measurement System

Four probe apparatus is one of the standard and most widely used methods for the measurement of resistivity. The advantage of using the four-probe method is that one can eliminate completely the contact resistance. The experimental set up consists of probe arrangement, sample, constant current source, container to keep liquid Nitrogen, Vacuum pump, Pressure gauge and a digital nanovoltmeter. In our set-up the temperature is varied steadily by moving the sample into (cooling) and out (heating) of a liquid nitrogen Dewar using a stepper motor assembly. The rate of translation of the sample determines the cooling/heating rate. Typically, a translation speed of 5 mm/h corresponds roughly to a temperature change of 2 K/min. The sample chamber contains helium gas at low pressure to provide temperature uniformity. The current and voltage sources employed are from KEITHLEY model no.6221 (current source) and 2182A (Nanovoltmeter). Resistivity of all the samples was measured at low temperature down to liquid Nitrogen temperature. Rectangular shape samples were cut out from the Pellet for these measurements. Since most of the samples were highly resistive in some cases current as low as 100 nA was used to record the voltage drop across the sample.

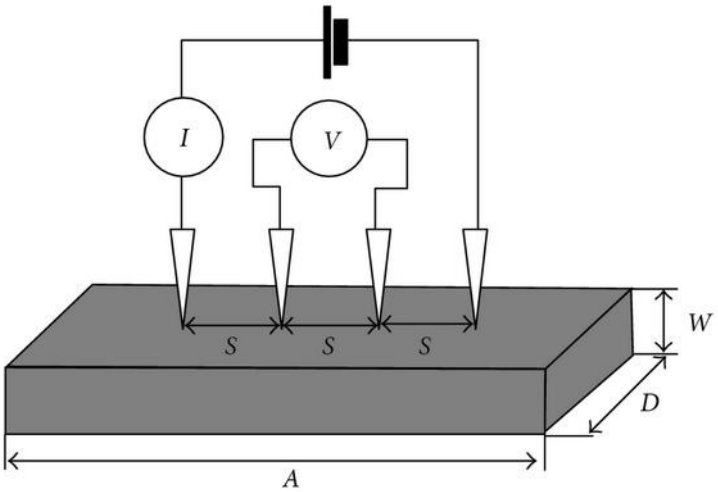

Figure 2.3: Schematic diagram of Four Probe Resistivity Measurement system. (Source: Wikipedia)

Chapter 3

Results & Discussion

3.1 Preparation of various $BaFeO_{3-\delta}$phases

The samples were prepared by the conventional solid state reaction route. Starting precursors were $BaCO_3$ (99.99% pure, Alfa Aesar) and Fe_2O_3 (99.98% pure, Alfa Aesar). The precursors were weighed according to the reaction equation given below:

$$4BaCO_3 + 2Fe_2O_3 + xO_2 \rightarrow 4BaFeO_{3-\delta} + 4CO_2$$

where x represents the undetermined amount of oxygen absorbed during the reaction, depending on the oxygen partial pressure in the sintering atmosphere. It is related to x by the relation $x = 1–2\delta$. The actual reaction mechanism need not be as simple as depicted above because of the presence of residual moisture, H_2 and CO gas in the sintering atmosphere; however, the ratio of the metal ions will be unaffected and will not interfere with the weighing of the starting precursors. The precursors were weighed accurately in their respective stoichiometric proportion and mixed thoroughly for around 45 mins by using a mortar and a pestle. Then, the mixture was kept in an alumina boat and was subjected to a heat treatment in air atmosphere at 1223 K for 24 h using a Naberthem muffle furnace. The mixture was then grounded thoroughly before pelletizing using an uniaxial hydrostatic press under 10 bar pressure. The pellet was sintered at 1323 K in air for 24 h and this process was repeated two to three times with an intermediate grinding.The resulting powder is called A on which subsequent heat-treatments were carried out under different conditions as explained below.

3.1.1 Synthesis of Hexagonal phase $BaFeO_{3-\delta}$

First, a part of the parent sample ‘A’ was divided into two batches named as ‘A1’ and ‘A2’. They were pelletized and subject to the following heat treatments: sample ‘A1’ was sintered at 1183 K for 24 h in the presence of 1 bar of flowing oxygen. Similarly, sample ‘A2’ was sintered at 1373 K for 24 h in presence of 1 bar of flowing oxygen. The heating and cooling rate in both cases was fixed at 450 K/h. Both reaction products were found to crystallize with the Hexagonal structure.

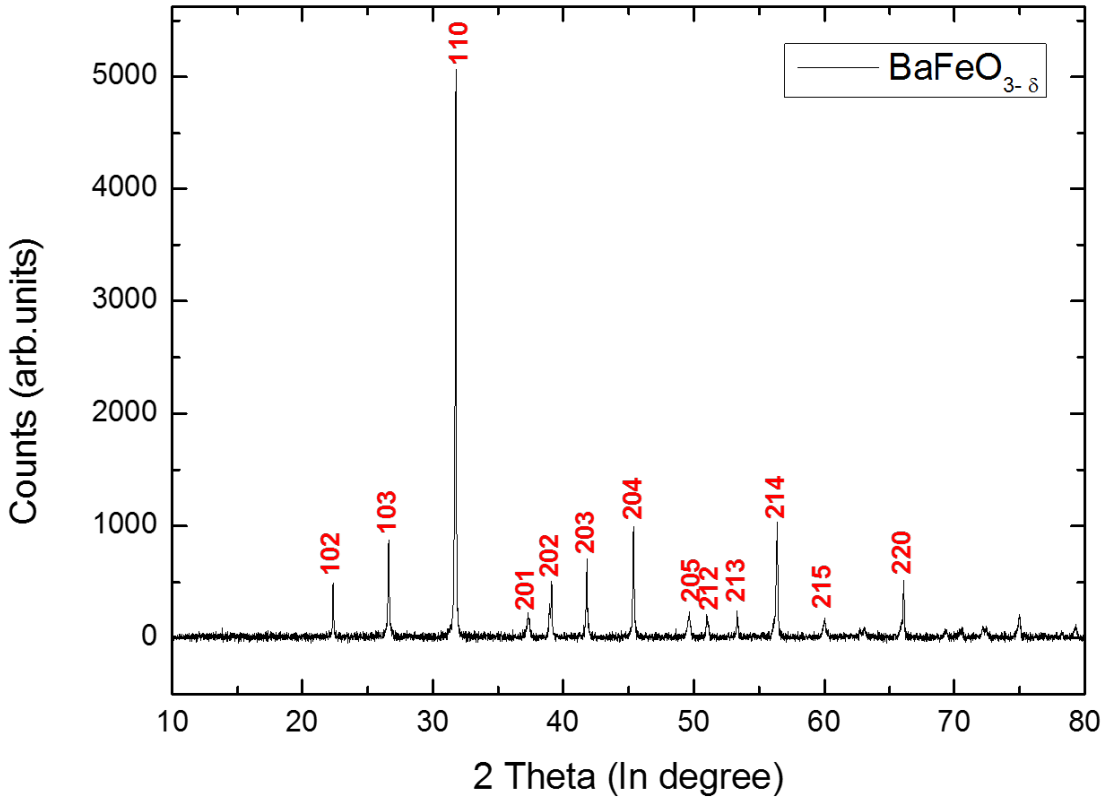

Figure 3.1: Shows the XRD plot of $BaFeO_{3-\delta}$ calcined at 1223 K, 1273 K, 1323 K in air and at 1323 K in presence of 1bar oxygen flow.

All the lines in the powder x-ray diffraction pattern could be indexed on the basis of the hexagonal structure reported in JCPDS 00-023-1024. The lattice parameter of the hexagonal phase was calculated using a freely downloadable program called UNITCELL and found to be a = $5.653A^0$, c = 13.876 A^0 and volume V = 382.22 A^{03}. These values are in good agreement with those reported in the literature [18,23]. It is well-know that the hexagonal phase forms with some oxygen deficiency. In fact, the fully oxygenated sample exhibits a cubic symmetry as reported recently and can only be prepared using ozone as an oxidizing agent. Attempts to obtain this phase under high pressure did not yield the desired results [23]. However, one can try increasing the oxygen content of the hexagonal phase by sintering it under high oxygen pressure which is something we plan to do in future. In the present investigations we did try to find out the effect of lowering the cooling rate on the stability of the hexagonal phase. The do so, we subjected the sample 'A2' to a further sintering at 1373 K for 24 h under a flowing oxygen stream at 1 bar of pressure. The cooling rate was set at 300 K/h, however, this resulted in the appearance of extra phases as shown in the figure below.

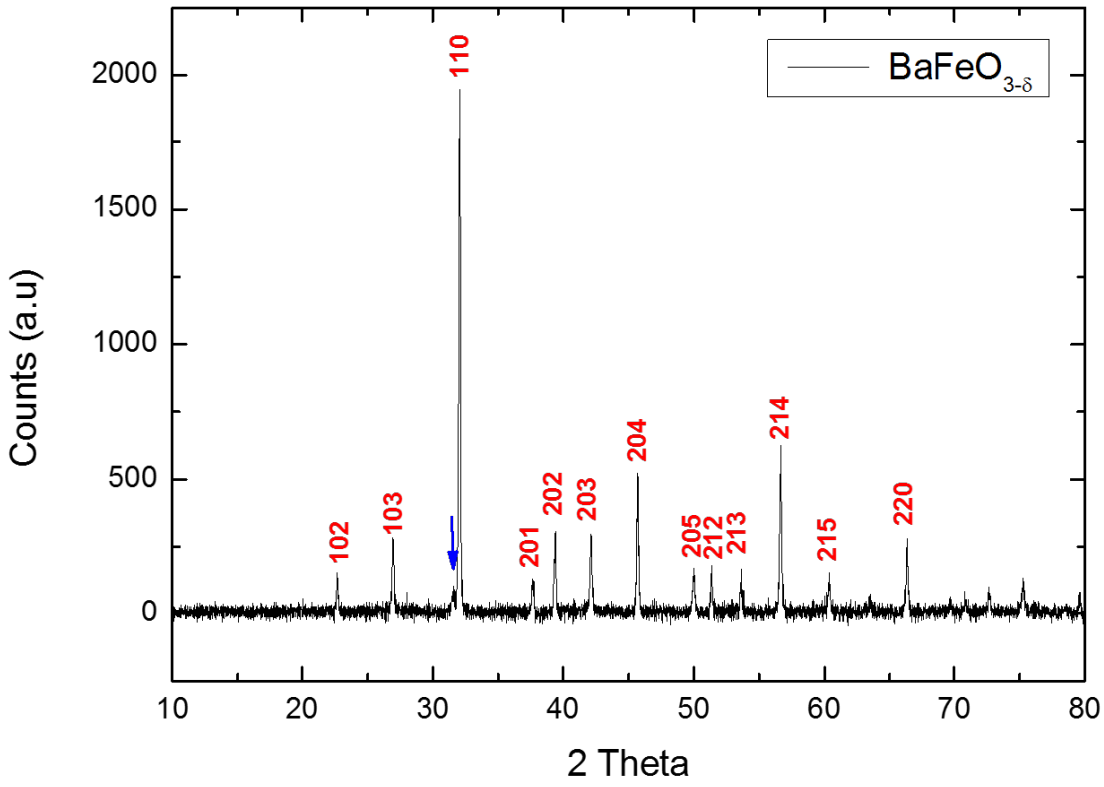

Figure 3.2: Shows the XRD pattern of $BaFeO_{3-\delta}$ under slow cooling.
Here the blue arrow represents the extra phase which corresponds to monoclinic phase.

3.1.2 Synthesis of Tetragonal phase of $BaFeO_{3-\delta}$

In a few previous reports it was reported that $BaFeO_{3-\delta}$ can be stabilized in a tetragonal phase.[18,23] . To get the tetragonal phase, a part of the sample 'A' was sintered under both air and oxygen separately for 12 hrs, each at 1273 K followed by rapid cooling of the sample by pulling it to one end of the tube furnace where the temperature is typically less than 350 K. The final reaction product (called A3) was analyzed using the powder x-ray diffraction which is shown in Fig. 3.3.

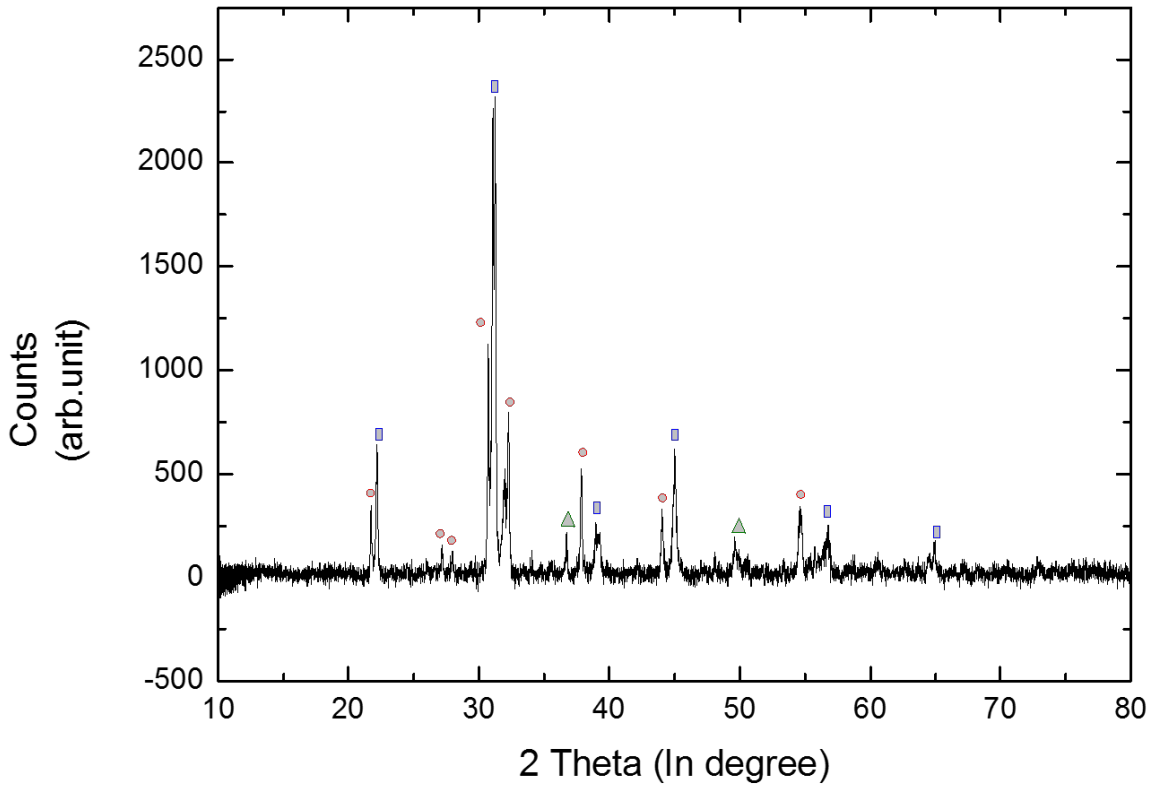

Figure 3.3: Shows the XRD pattern of Tetragonal $BaFeO_{3-\delta}$ with some impurity phases. Red Circle: Monoclinic Phase, Blue Rectangle: Tetragonal Phase, Green Delta: Hexagonal Phase

However, the resulting reaction mixture was found to be multiphase consisting of peaks corresponding the tetragonal phase (JCPDS 00-023-1023) with few additional peaks due to hexagonal and monoclinic phases

3.1.3 Synthesis of the Brownmillerite phase $Ba_2Fe_2O_5$

A part of sample 'A' was sintered at 1273 K for 12 h in the presence of 1 bar oxygen flow and subsequently cooled down very quickly by pulling the alumina boat to one of the tube furnace. In a subsequent step, the sample after regrinding and pelletizing was quenched from 1473 K in presence of air resulting in the formation of the monoclinic phase with Brownmilleirte structure. The powder x-ray diffraction of the resulting product is shown in the figure below.

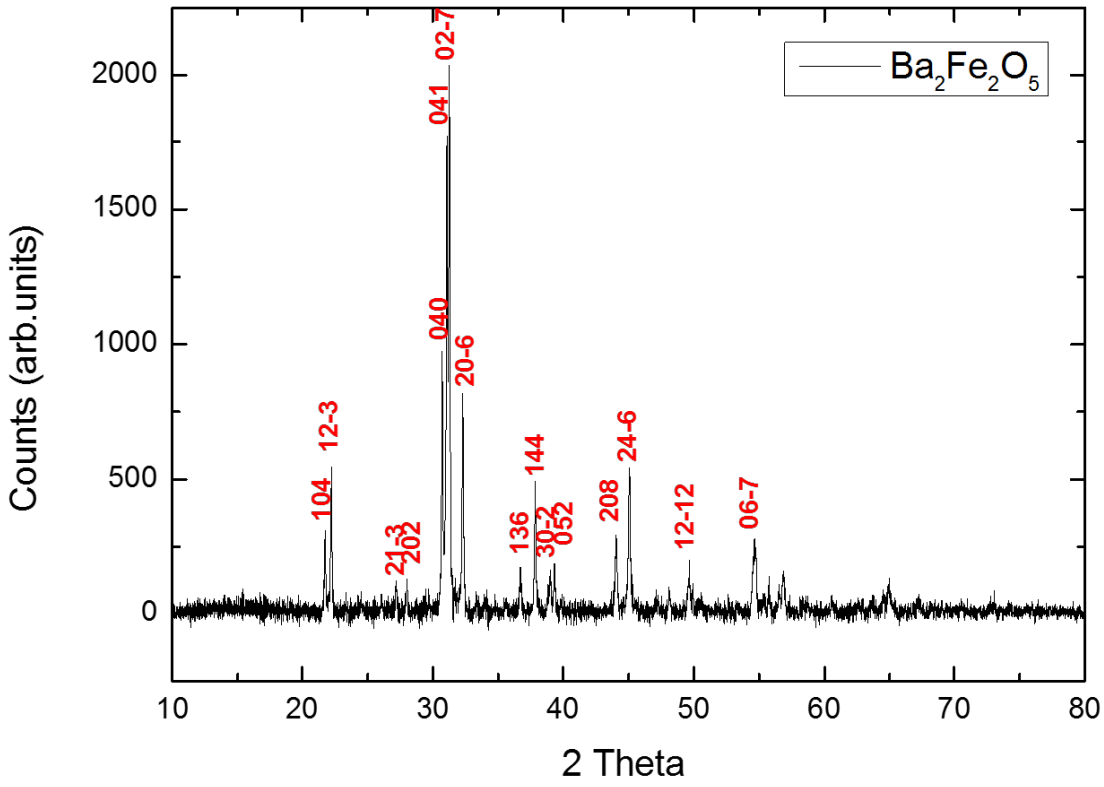

Figure 3.4: Shows the XRD pattern of Brownmillerite $Ba_2Fe_2O_5$ calcined at 1223 K, 1273 K, 1323 K in air and then quenched from 1323 K in oxygen flow and the again quenched from 1273 K in presence of air.

The pattern could be nicely indexed on the basis of the Brownmillerite structure reported in JCPDS (00-039-1296) with no extra peak indicating that the sample is of high purity. The lattice parameters of $Ba_2Fe_2O_5$ were calculated using the UNITCELL program are a = $6.929A^0$, b =$11.704\ A^0$, c = $23.131A^0$, V = $1875.85A^{03}$ and $\beta = 98.74^o$. These values are in good agreement with the corresponding JCPDS file.

3.1.4 Synthesis of La doped $BaFeO_{3-\delta}$

The precursors taken for the preparation of La doped $BaFeO_{3-\delta}$ were $BaCO_3$ (99.99% Pure, Alfa Aesar), Fe_2O_3 (99.98% Pure, Alfa Aesar), La_2O_3 (99.99% Pure, Alfa Aesar). The stoichiometric quantities of the precursors were taken to synthesize $Ba_{1-Y}La_YFeO_{3-\delta}$ for Y = 0.02, 0.04, 0.06, 0.08, 0.1, 0.2, 0.3, and 0.4.The precursors were taken according to the reaction equation given below.

$$2(1-Y)BaCO_3 + Fe_2O_3 + (Y)La_2O_3 \rightarrow Ba_{1-Y}La_YFeO_{3-\delta} + (1-Y)CO_2 + (1-\frac{Y}{2})O_2$$

The starting precursors were weighed and mixed thoroughly using a pestle and a mortar. Due to the hygroscopic nature of Lanthanum Oxide (La_2O_3), it was preheated

at 1173 K before weighing. The mixture were loaded in an alumina boat and sintered at 1223 K for 24 h in the presence of air. The powder thus obtained was well grounded and pelletized. These pellets were sintered at 1323 K with an intermediate grinding. The heating and cooling rate was fixed to be 450 K/h in all the cases. Finally, all the samples were subjected to a heat treatment at 1373 K in presence of 1 bar oxygen flow for 24 h. For reasons mentioned later, we re-sintered a part of the samples doped with 1% and 2 % La at 1373 K, however, unlike the previous sintering step, here the samples were allowed to cool relatively slowly at 300 K/h to room temperature in presence of 1 bar oxygen flow. The reaction product sintered at 1373 K and cooled to room temperature at 450 K/h indicated the formation of the hexagonal phase but the presence of some impurity phase(s) were also observed. However, the subsequent sintering at 1373 K where the samples were cooled relatively slowly (300 K/h) proved efficient in eliminating the extra phase completely within the resolution limit of powder X-ray diffraction technique. XRD pattern of 1% La doped $BaFeO_{3-\delta}$ is given in figure 3.5.

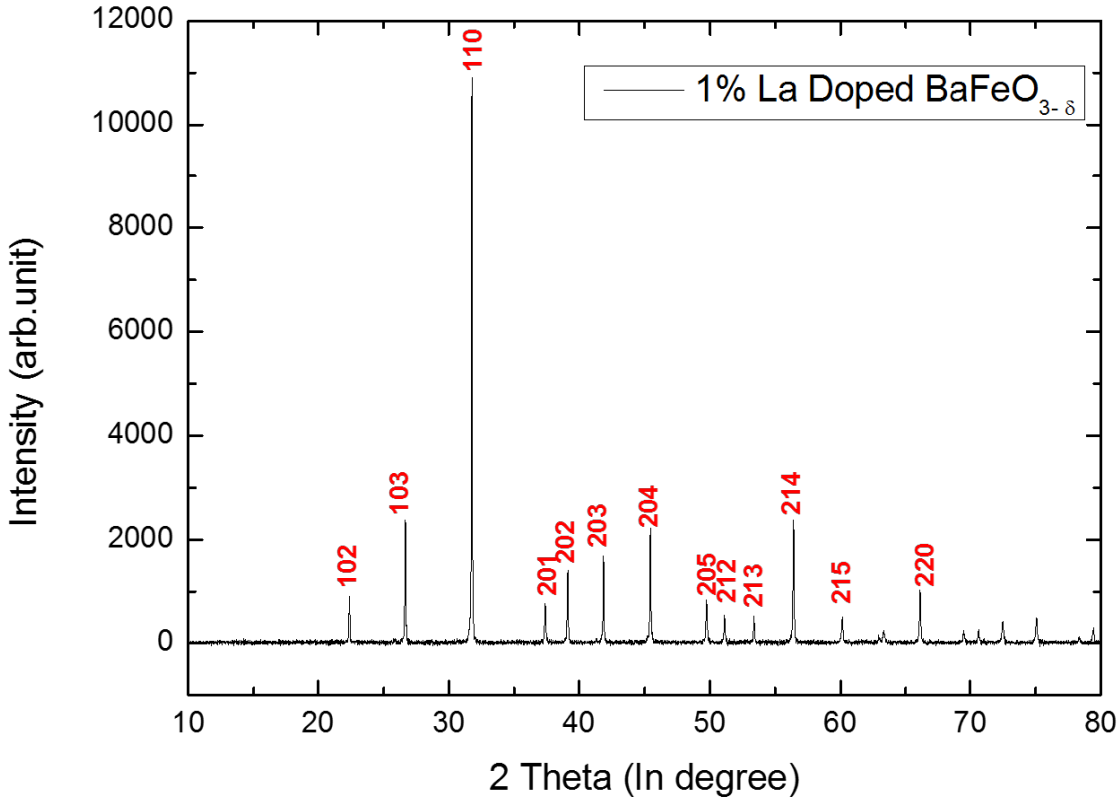

Figure 3.5: Illustrates the XRD pattern of 1% La doped $BaFeO_{3-\delta}$ calcined at 1223K, 1273K, 1323K in air. Then calcined at 1373 K in presence of oxygen with a normal cooling rate and again sintered at 1373 K in presence of oxygen with a very slow cooling rate.

A comparison of the obtained x-ray diffraction pattern with that of the standard pattern for the hexagonal phase reported in JCPDS 00-023-1024 agreed very well. Lattice parameter as well as unit cell volume were calculated and are found to be a= 5.614A^0, c=

13.622A^0 and V= 370.53 A^{03} . The X-ray diffraction plot of 2% La doped $BaFeO_{3-\delta}$ is shown in figure 3.6.

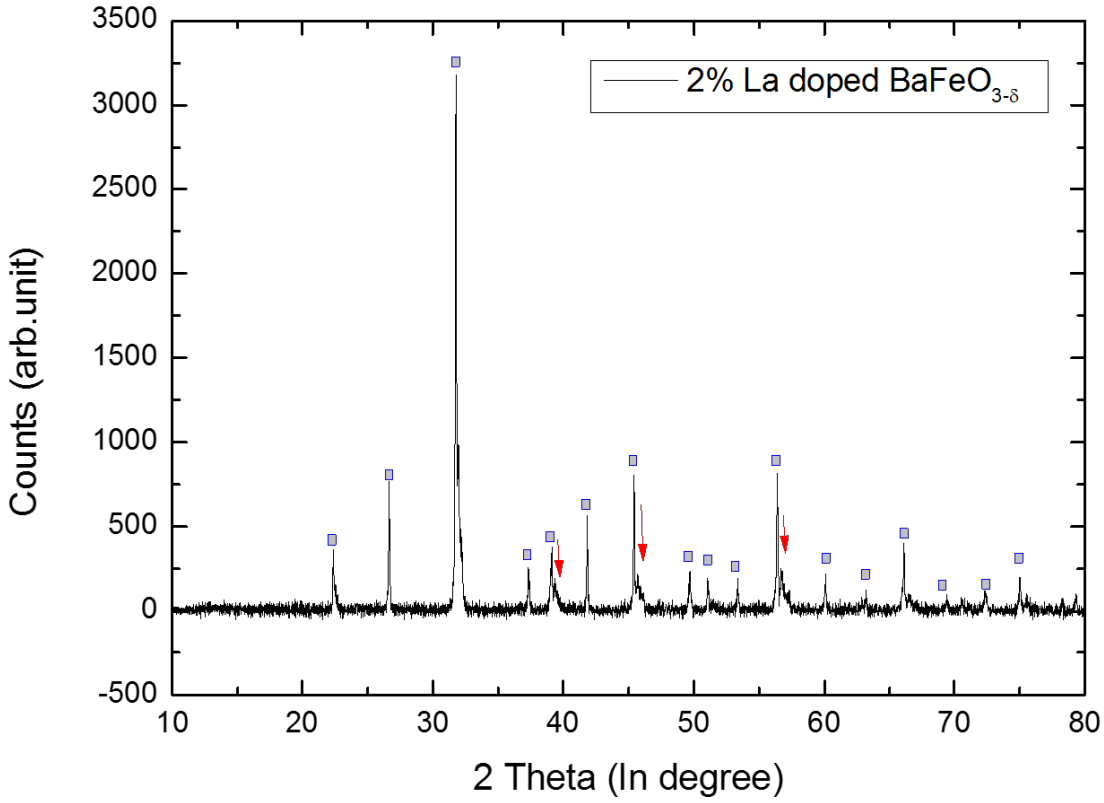

Figure 3.6: Shows the XRD pattern of 2% La doped $BaFeO_{3-\delta}$ with some impurity phase. (Arrow mark shows the impurity peaks)

The main diffraction peaks could be indexed on the basis of the hexagonal structure, however, several small extra peaks (indicated by arrow) were also present. Even the sintering step at 1373 K followed by slow cooling as mentioned above could not help in eliminating or reducing the intensity of these extra peaks. These extra lines are likely due to the competing tetragonal phase which is getting stabilized due to the incorporation of La at the Ba site. This is rather apparent from the fact that for sample with higher La concentration the volume fraction of the tetragonal phase increased and eventually for a sample with 20 % La doping the volume fraction of the tetragonal phase reached almost 100 % as shown in the x-ray diffraction pattern of this sample in Fig. 3.7. All the diffraction lines could be nicely indexed based on the tetragonal structure of $BaFeO_{3-\delta}$ reported in JCPDS 00-023-1023.

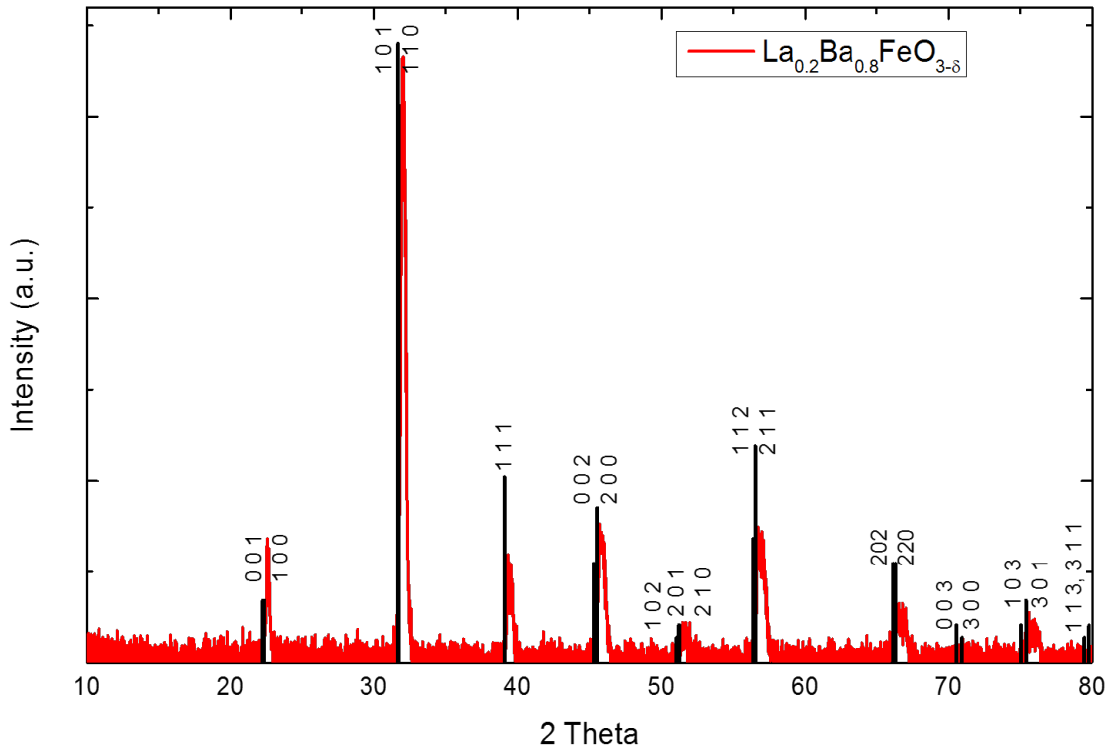

Figure 3.7: Shows the XRD pattern of 20% La doped $BaFeO_{3-\delta}$

3.1.5 Stabilization of Cubic phase of $BaFeO_{3-\delta}$

Since the structure of no oxygen deficient $BaFeO_{3-\delta}$ (i.e, $\delta = 0$) is reported to be cubic, we tried to stabilize the cubic by doping Sr, Ca and Y at the Ba site. This work is motivated by a recent report by Dong et al. where they showed that 5% La doped $BaFeO_{3-\delta}$ can be stabilized in the cubic phase [1]. We prepared samples with 5% Sr, Ca and Y substitution at the 'Ba' site. Following the method of Dong et al., we sintered these samples at 1273K in air for 24 h followed by a subsequent sintering at 1273K in 1 bar oxygen flow for 24 h with an intermediate grinding. However, the reaction products were found to be multiphased samples consisting of a mixture of Tetragonal, Hexagonal and Monoclinic (Main phases). In a subsequent step, the samples were quenched from 1273K in presence of oxygen flow, still the cubic phase didn't form. These negative results prompted us to verify the results due to Dong et al. by doping 5% La at the Ba site and following the same sintering procedure as mentioned in their paper. However, the X-ray diffraction pattern of the resultant product, as shown in figure 3.8 showed mixed phases as for the case of Sr, Ca and Y.

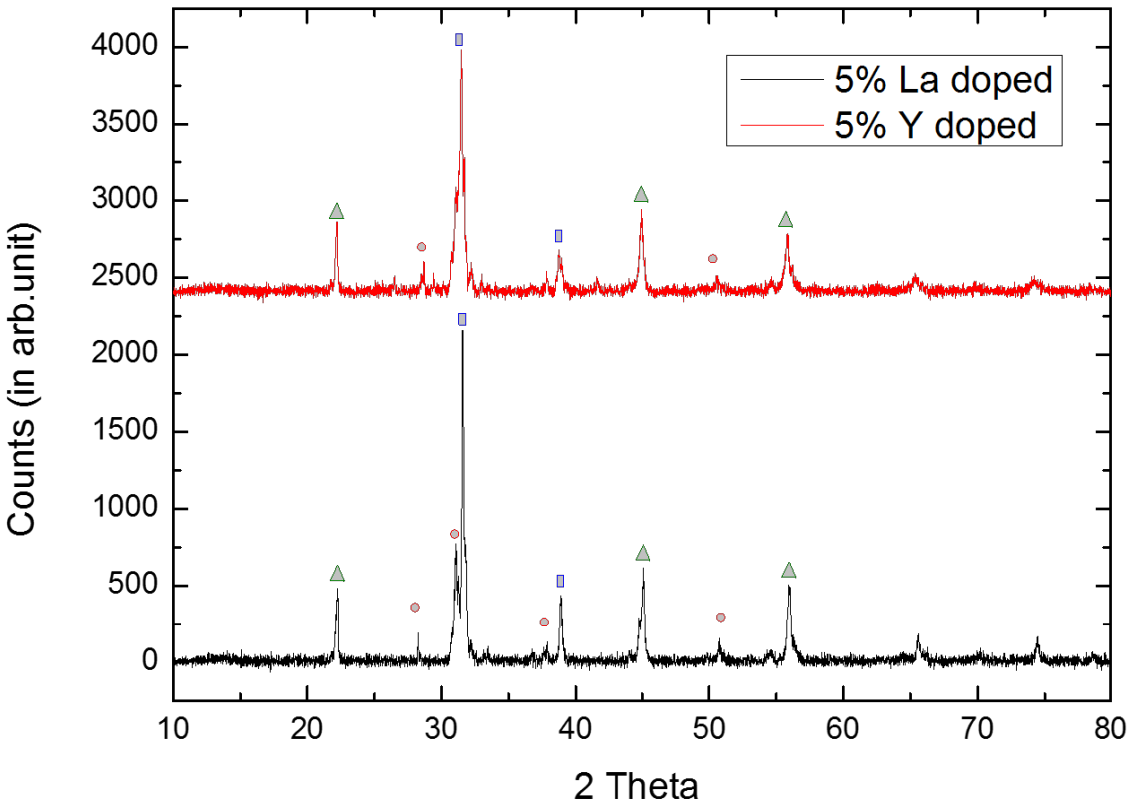

Figure 3.8: Shows the XRD pattern of 5% 'La' and 'Y' doped $BaFeO_{3-\delta}$ with some impurity phases.
Delta : Hexagonal phase, Circle : Monoclinic phase, Rectangle : Cubic/ Tetragonal phase

Here, it must be mentioned that the X-ray diffraction pattern of the cubic (JCPDS 01-075-0426) and the tetragonal (JCPDS 00-023-1023) phases have subtle difference and distinguishing them from a qualitative comparison is rather difficult (the lattice parameter of Cubic $BaFeO_3$ and tetragonal $BaFeO_{3-\delta}$ differs only marginally). Therefore, one can completely rule out the formation of the cubic phase along with some small impurity peaks of the hexagonal and monoclinic phases.

3.1.6 Synthesis of single crystal of $Ba_2Fe_2O_5$

For the crystal growth experiments, polycrystalline feed rod of composition $Ba_2Fe_2O_5$ was prepared by conventional solid state reaction route which is already discussed in subsection 3.1.3. The feed rod was prepared by filling the powder, which was obtained after the final round of heat treatment, in a rubber tube and cold-pressed under 700 bar isostatic pressure. The compactified rod was further densified by heating at 1473 K for 24 h. In the first growth experiment, lamps of 1000 W were used. However, the floating zone was difficult to stabilize and it broke on several occasions probably because the length of floating zone was too large further the diameter of the grown crystal or of the feed rod. Therefore, in the subsequent growth experiment we used 150 W lamps which have

very narrow filament resulting in a tight focusing of the infrared radiations. With these smaller lamps the float-zone could be successfully stabilized over the entire duration of the growth experiment. The values of the various parameters used during these growth experiments are summarized in table no 3.1.

	v_f^a **(mm/h)**	v_g^b **(mm/h)**	ω_L **rpm**	ω_U **rpm**	**Lamp W**	**Power (%)**	**Growth length mm**
Exp. 1	5	5	30	30	1000	38.6	55.3
Exp. 2	5	5	30	30	150	70	72.77

Table 3.1: Summary of growth parameters. v_f^a- Feeding speed, v_g^b- Growth speed, ω_L- Rotation speed of Lower part, ω_U- Rotation speed of Upper part

Images of the single crystal (Both obtained by experiment 1 nad 2) are shown in fig.3.9 and 3.10 respectively

Figure 3.9: The grown crystal boule of $Ba_2Fe_2O_5$(experiment 1)

Figure 3.10: The grown crystal boule of $Ba_2Fe_2O_5$(experiment 2)

To investigate the compositional and structural homogeneity of the grown crystal, small sections were cut at different lengths of the crystal boule for optical microscopy under polarized light and powder XRD diffraction. This work is ongoing and here we show our powder XRD results of crystal grown during the first trial.

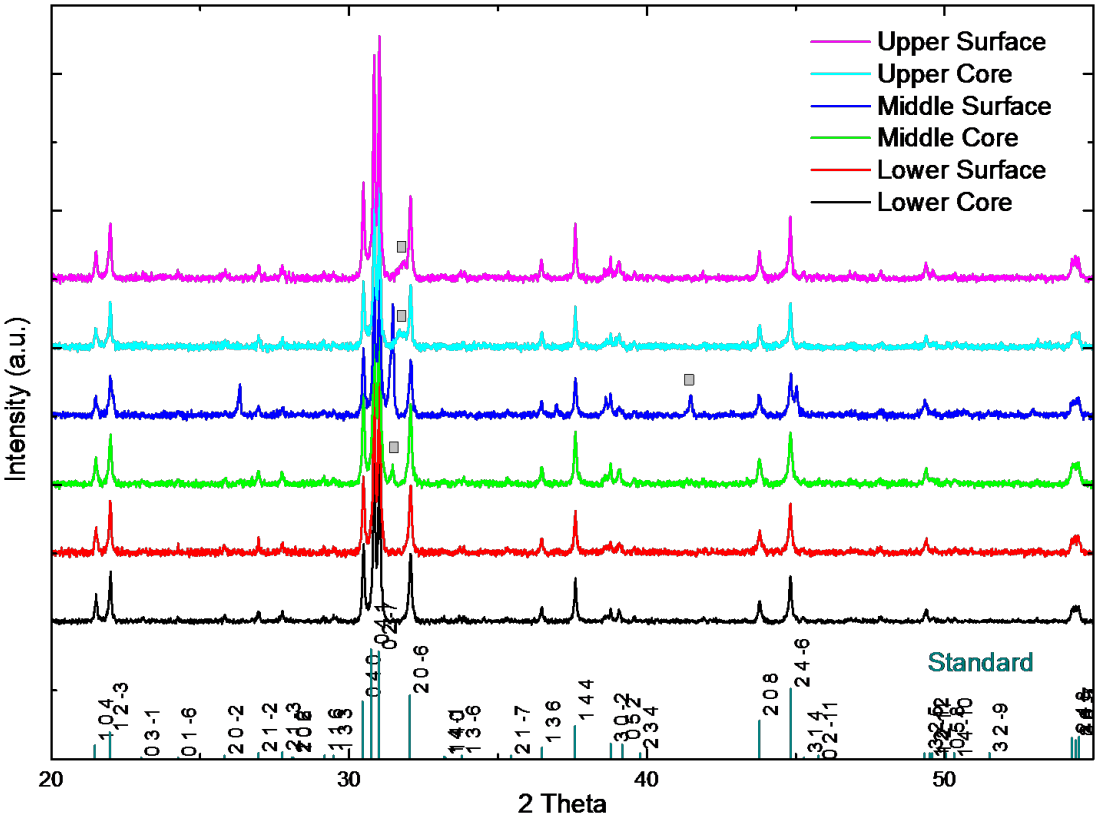

Figure 3.11: XRD pattern of different sections of the grown crystal of $Ba_2Fe_2O_5$(Experiment 1). Here, "upper", "middle" and "lower" refer to the positions of the investigated sections with respect to the starting of the growth experiment. Square: represents the impurity phase.

From the XRD pattern recorded at different lengths of the crystal, it was observed that in the lower part, i.e., 1 cm from the starting of the growth experiment (for powder obtained from both the core and surface regions of the section) , pure $Ba_2Fe_2O_5$phase has been crystallized. However, in the middle (4 cm) and the upper (5.5 cm) sections the hexagonal impurity phase and an unidentified phase also crystallized. The lattice parameters of the lower crystal section calculated using the UNITCELL program are: a= 6. 937 A^0, b= 11.713 A^0, c= 23.264 A^0, V= 1890.41 $A^{03}$and $\beta = 98.54^0$in excellent agreement with the literature (JCPDS 00-039-1296). For the crystal grown during the second experiment the structural characterization is under progress.

3.2 SEM Analysis

Representative SEM images of the samples $BaFeO_{3-\delta}$, 1% La doped $BaFeO_{3-\delta}$, 20% La doped $BaFeO_{3-\delta}$ and $Ba_2Fe_2O_5$ are shown in figure 3.11(a),3.11(b),3.11(c),3.11(d), respectively. The microstructure of all the specimen shows grains of various morphologies and sizes. From the images it appears that the grain size decreases with increasing La concentration and for 20 % La-doped sample the grain size distribution appears to be

more homogeneous. In the $Ba_2Fe_2O_5$, which is sintered at relatively higher temperature (1473 K) the grains appeared to have agglomerated.

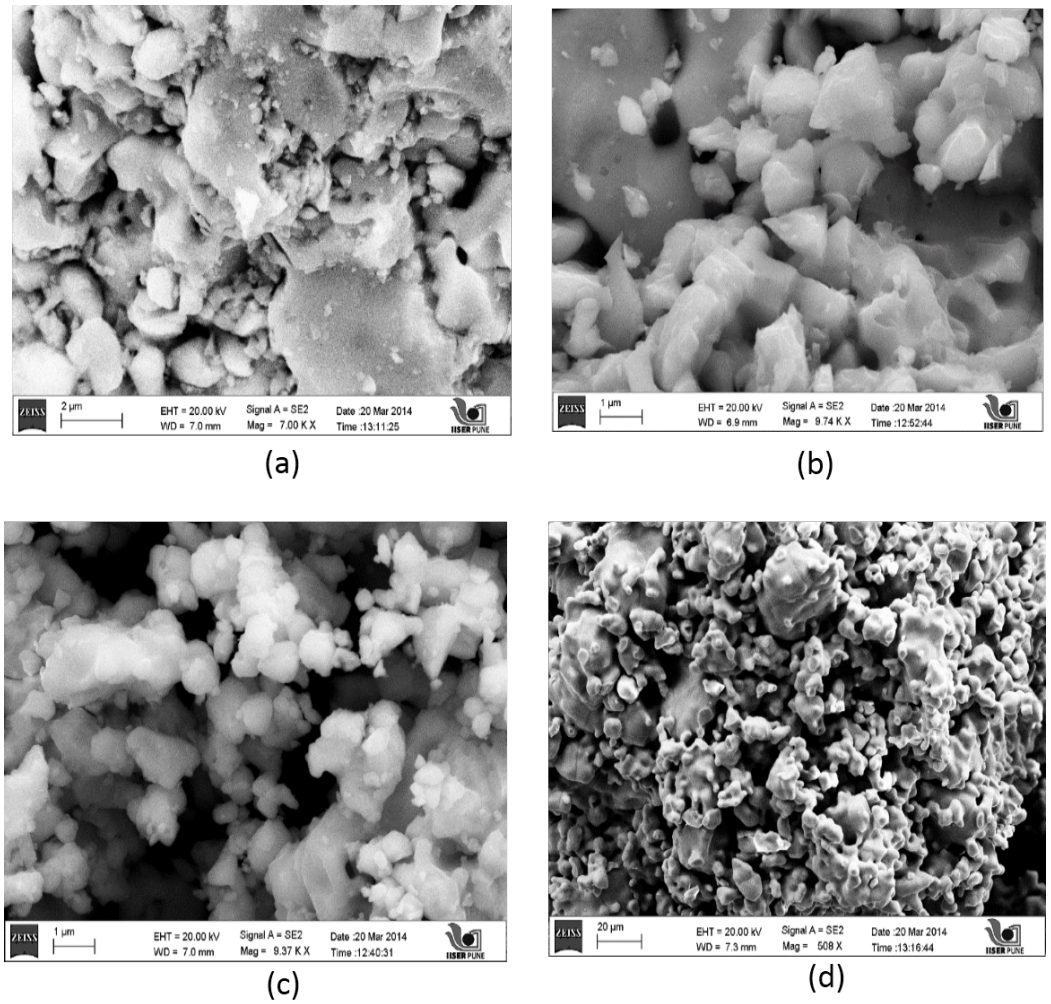

Figure 3.12: Surface morphology using SEM for (a) $BaFeO_{3-\delta}$ (b) 1% La doped $BaFeO_{3-\delta}$ (c) 20% La doped $BaFeO_{3-\delta}$ (d) $Ba_2Fe_2O_5$

3.2.1 EDAX Analysis

Elemental analysis of these specimens was carried out using the EDAX tool attached to the SEM at 20 KeV accelerating voltage. The EDAX results for 1% La doped $BaFeO_{3-\delta}$,$BaFeO_{3-\delta}$, $Ba_2Fe_2O_5$and 20% La doped $BaFeO_{3-\delta}$ are shown in figure 3.12(a), 3.12(b), 3.12(c), 3.12(d) respectively.

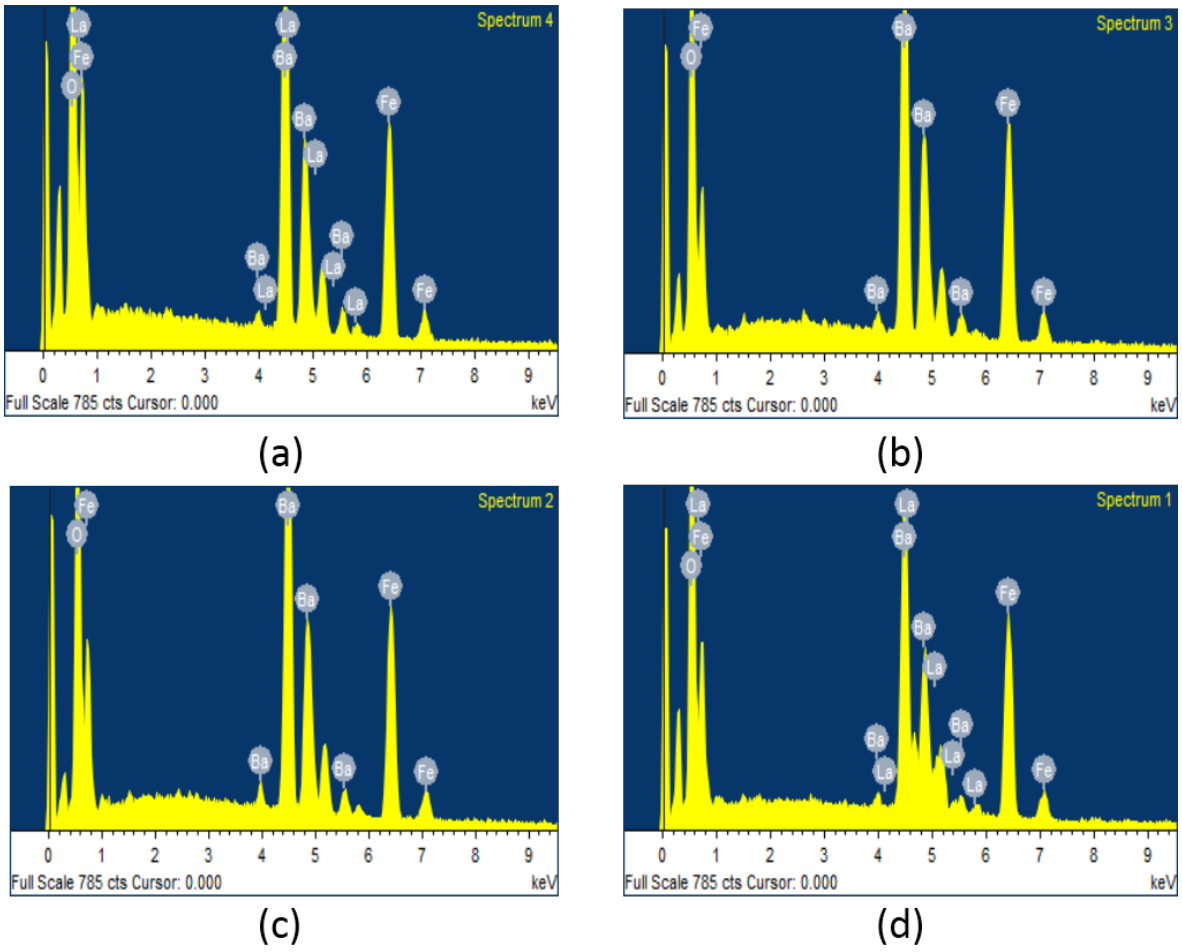

Figure 3.13: EDAX of (a)1% La doped $BaFeO_{3-\delta}$ (b) $BaFeO_{3-\delta}$ (c)$Ba_2Fe_2O_5$ (d) 20% La doped $BaFeO_{3-\delta}$

The quantitative results of EDAX are presented in the table below.

Compounds	At. ratio of Ba w.r.t Fe	At. ratio of La w.r.t Fe
$BaFeO_{3-\delta}$	1.04	-
1% La doped $BaFeO_{3-\delta}$	1.00	0.03
20% La doped $BaFeO_{3-\delta}$	0.86	0.21
$Ba_2Fe_2O_5$	1.04	-

Table 3.2: Shows the atomic composition of different elements in all the compounds

Briefly, the compositions obtained using EDAX are found to be in very good agreement with the nominal compositions.

3.3 Physical properties

3.3.1 Magnetization

The dc-susceptibility χ of the powdered samples of the hexagonal $BaFeO_{3-\delta}$ and 20% La doped $BaFeO_{3-\delta}$ were measured as a function of temperature using a Quantum de-

sign PPMS. The amount of sample weights taken for these measurements were 0.047 g and 0.045 g for $BaFeO_{3-\delta}$ and 20% La doped $BaFeO_{3-\delta}$, respectively. The magnetic measurements were carried out under applied magnetic fields ranging from 100 Oe to 1 KOe. The temperature dependence of the susceptibility under the zero-field-cooling (ZFC) and field-cooling (FC) conditions for $BaFeO_{3-\delta}$ is shown in figure 3.13. Besides a large thermomagnetic irreversibility indicative of magnetic relaxation processes several notable features were observed in the temperature dependence of the magnetic susceptibility. Upon cooling below room temperature the ZFC susceptibility shows a weak anomaly around T = 250 K and a prominent peak near T = 160 K. Upon further cooling the sample, the susceptibility decreases rapidly becoming negative around T = 125 K and in the negative region (below about T = 110 K) ceases to decrease as rapidly as it did above this temperature, indicating a cross-over from one magnetic state to another. These features at T = 250, 170 and 110 K are also seen in the FC susceptibility and are shown by arrows in fig. 3.14.

To get an insight into what might possibly be happening at these temperatures, we measured the isothermal magnetization (IM) of our sample at temperatures T = 310 K, 200 K, 80 K and 2 K. Before measuring the IM at any temperature the sample is cooled from 310 K in a nominal zero-field to that temperature.

The T = 310 K IM is characterized by a linear variation of magnetization up to the highest applied field of 80 KOe, suggestive of a paramagnetic state. In the paramagnetic state, IM should follow the Brillouin function dependence. The magnetization calculated using the Brillouin function gives a value of roughly 800 emu/Fe^{4+} at T = 300 K under 80 KOe. The observed value of about 650 emu/mol at T = 310 K and 80 KOe is in a reasonable agreement. Since the hexagonal phase is oxygen deficient [18,19], one would naturally expect the presence of Fe^{3+} in the sample which can be in a high-spin (S= 5/2), intermediate-spin (S = 3/2) or low-spin state (S = 1/2). In the high-spin state, the magnetization per Fe^{3+} at 300 K and 80 KOe is about 1160 emu; in the intermediate state this value of about 500 emu and in the low-spin state about 100 emu. Clearly, the observed value of 650 emu/mol cannot be understood from the high-spin state. Assuming intermediate spin state, a hand-waving calculation (800 $\times$ mol fraction of Fe^{4+} +600 $\times$ mol fraction of Fe^{3+} = 650 emu) yields a value of about 50 % for Fe^{3+} mol fraction which is too large to be true. However, a similar calculation assuming low-spin gives a value of 21 % of Fe^{3+}, which is quite reasonable and provides a good estimate of the stoichiometry to be $BaFeO_{2.89}$, in good agreement with previous reports where the stoichiometry of the hexagonal phase is measured using thermogravometric or iodometric titration methods [18,20].

The IM at T = 200 K deviates from linearity, suggesting that the anomaly at 250 K corresponds to a transition into some kind of an ordered moment state. To understand what this ordered state could be we notice that the magnitude of magnetization under 80 KOe has now increased to roughly three times its value at room temperature and a minor but clearly discernable hysteresis loop appears in the magnetization as shown in the inset of the corresponding figure. These observations indicate that a weak ferromagnetic state sets-in below about T = 250 K with a canted spin structure. The peak at T = 170 K, could possibly be due to spin-reorientation which is one of the characteristic magnetization features of rare-earth based orthoferrites with canted spin structure that arises due to antisymmetric Dzyaloshinskii-Moriya type interaction $\boldsymbol{D}.\ (\boldsymbol{S_i}\ \mathrm{x}\ \boldsymbol{S_j})$ [46]. These features also manifests themselves in the IM measured at T = 80 K and 2 K.

The T = 80 K data shows pronounced curvature and larger magnetization under 80 KOe (approximately twice the value at T = 200 K), moreover, the size of the hysteresis loop has also become relatively larger now, showing that the possible spin-reorientation below T = 170 K has gradually changed the canted spin structure to a somewhat simpler spin structure. The magnetization at T = 2 K doesn't really differ much from that at T = 80 K as far are the magnitude is concerned, showing no further changes in the magnetic structure at low temperatures. An increase of the width of the hysteresis loop at T = 2 K is due to pinning barrier height being larger than the thermal energy. Interestingly, a part of the virgin curve in the M-H loop lies outside the hysteresis loop. The exact cause for this behavior is as yet unclear. Although unusual, such an effect can arise in magnetic system with first-order magnetic transition [47].

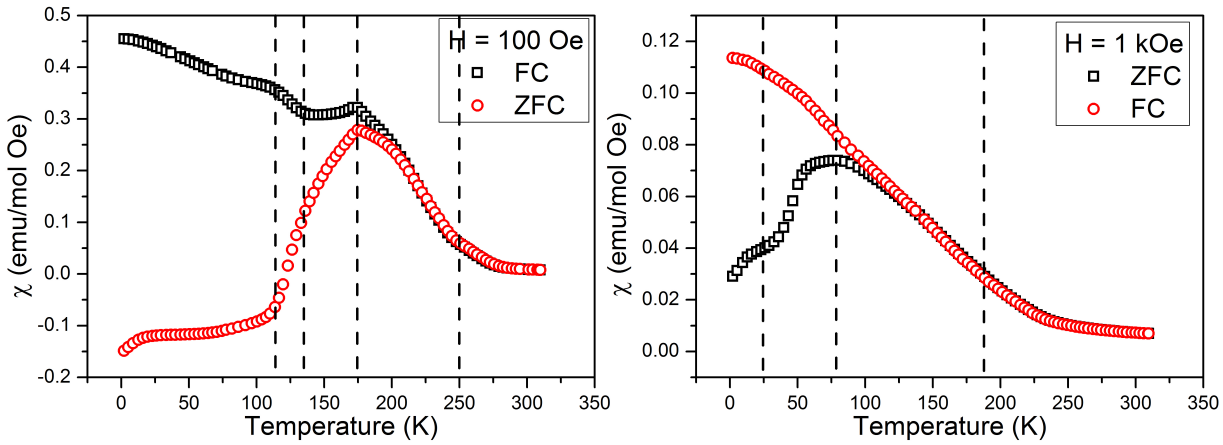

Figure 3.14: shows the temperature dependence magnetic susceptibilities of $BaFeO_{3-\delta}$and 20% La doped $BaFeO_{3-\delta}$respectively. Black square: Zero field cooling.

Doping with trivalent Lanthanum at the divalent Barium site implies further increase in Fe^{3+} in the structure. Since the actual oxygen content of the La doped sample may differ from the undoped sample the increase in Fe^{3+} need not be equal to the amount of La^{3+} substituted. What is known from the literature is that rare-earth orthoferrites are nearly stoichiometric; therefore, La-doped sample should have relatively higher oxygen content than its undoped counterpart. In fact, if we assume 20 % La doped sample to be exactly stoichiometric then its Fe^{3+} content would be roughly equal to that of $BaFeO_{2.89}$ (the estimated stoichiometric of our undoped sample), however, since doping with La, results in a decrease of resistivity (discussed in the next section), it seems that La^{3+} doping does lead to electron doping or in equivalent terms an increase of the Fe^{3+} contents per formula unit. The temperature dependence of the susceptibility of 20% 'La' doped$BaFeO_{3-\delta}$ is shown in figure 3.14. χ(T) exhibits a broad maximum centered around T = 70 K. Below this temperature the χ(T) behavior is rather similar to that of the undoped sample. The susceptibility of two samples near room-temperature, in the paramagnetic regime, is nearly equal. The change of slope of χ(T) near T = 225 K, below which a region of somewhat steeper increase of χ(T) ensues, is similar to the behavior of its undoped counterpart. Thus, judging from the bulk magnetic response, the overall behavior of the two samples seems to agree well except for a shift of the temperature scale with anomalies in doped sample appearing at lower temperatures compared to the

undoped sample. The IM of the doped samples were carried out at T = 200, 70 and 2 K (Fig. 3.16). The overall behavior of IM is also similar to the undoped counterpart albeit with less amplified features. For instance, here the virgin curve lies very close to the hysteresis loop. The magnitude of magnetization at T = 2 K under 80 KOe is around 1750 emu/mol which is less than the undoped sample under the conditions. Possible reason for this decrease could be a significant increase of low-spinFe^{3+} moments in the doped sample.

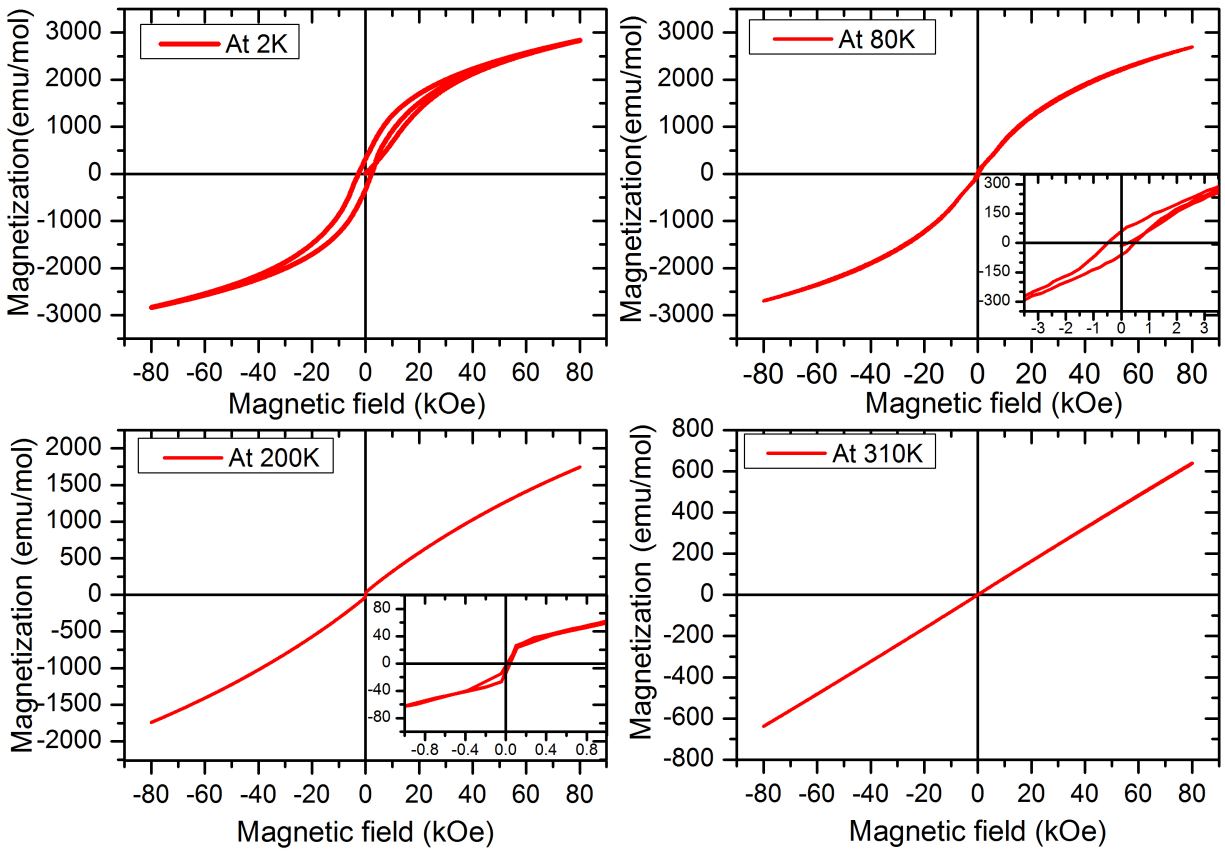

Figure 3.15: Hysteresis loop of $BaFeO_{3-\delta}$ at different temperatures.

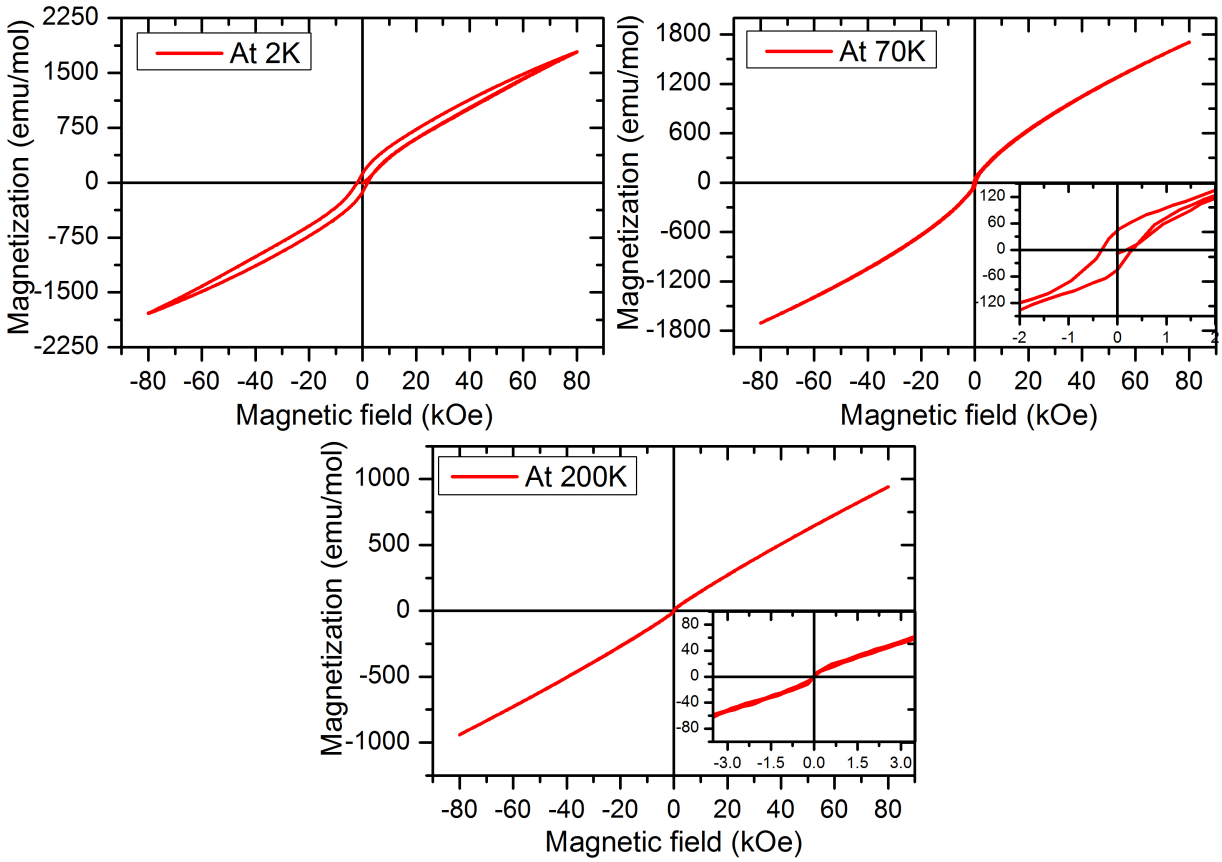

Figure 3.16: Hysteresis loop of 20% La doped $BaFeO_{3-\delta}$ at different temperatures.

3.3.2 Electrical resistivity

The temperature variation of electrical resistivity of 1 % and 20 % La doped samples is shown in figure 3.17. Attempts to measure the undoped sample were proved unsuccessful due to its highly resistive nature. The room temperature resistivity of the two samples were measured to be: 0.5 MΩ (1 % La) and 328Ω (20 % La). Upon decreasing the temperature the resistivity of the two samples continuously increases. However, for the 1 % La doped sample the rate of increase is substantially higher. As seen in the figure below, at temperatures less than T = 180 K, the resistivity increases very steeply increasing from a value of about 2 MΩ at 180 K to almost 200 MΩ near 155 K below which it became impossible to measure it even at the lowest current used (~ 100 nA). On the other hand, the resistivity of 20 % La doped sample remained less than 1 MΩ down to 120 K, below this temperature a sharp increase is recorded with a value of about 80 MΩ at the lowest measurement temperature (85 K). A kink in the resistivity is observed near T = 90 K in both heating and cooling data. It may be related to the broad magnetic anomaly centered on T = 70 K. However, at this point of time, we will refrain ourselves from assigning any definitive interpretation to it.

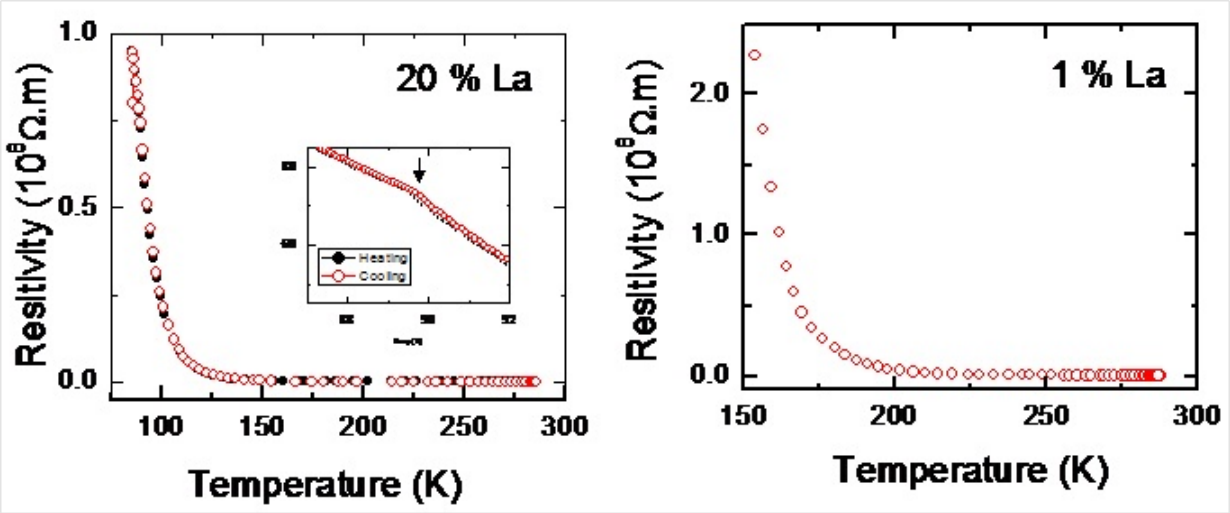

Figure 3.17: Resistivity measurement of 20% La doped $BaFeO_{3-\delta}$and 1% La doped $BaFeO_{3-\delta}$

Chapter 4

Conclusions & Outlook

We have successfully synthesized polycrystalline samples of $BaFeO_{3-\delta}$ with hexagonal and monoclinic structures. The tetragonal structure type could not be obtained as a single phase. The effect of Ca, Sr, La and Y doping at Ba site is investigated. It was found that La and Y substitution tends to stabilize the cubic or the closely related tetragonal structure. We also investigated the effect of La-substitution by systematically increasing the La percentage. We show that while the 1 % La-doped sample retains the hexagonal structure of the undoped counterpart, with increasing La substitution, multiphase hexagonal/tetragonal sample results with increasing tetragonal and decreasing hexagonal volume fraction. Near 20 % substitution the entire sample transforms to a single-phase tetragonal structure. Single-crystals of the Brownmillerite phase is grown using the floating-zone method associated with a four-mirror image furnace. Magnetization measurements were performed on $BaFeO_{3-\delta}$ (hexagonal) and its 20 % La-doped $BaFeO_{3-\delta}$ (tetragonal) samples. Both samples show weak ferromagnetism at low temperatures as inferred from minor hysteresis loops in the isothermal magnetization measured at T = 2 K. The temperature variation of the zero-field-cool magnetization of the 'pure' sample exhibits a peak near T = 170 K, below this temperature, the magnetization decreases rapidly becoming negative below about T = 120 K. In contrast, magnetization of the La-doped sample shows a rather broad peak centered at T = 70 K. Upon cooling below this temperature the susceptibility decreases rapidly but does not become negative. The resistivity measurements show an increase of the electrical conductivity due to the electron-doping in the La-doped samples.

Future plans: The results obtained so far are very interesting and encourage us to continue this work further so that some key questions can be answered and more light can be shed on the formation and stability regimes (in terms of oxygen contents) of the various structure variants of$BaFeO_{3-\delta}$. In the near future our plan is as follows: 1. To develop an iodometric technique to determine the actual oxygen content of our samples (typical iodometric technique rely on reducing Fe^{3+} to Fe^{2+}, however, our samples contain an overwhelming amounts of Fe^{4+}). 2. To carry out systematic magnetic measurements on samples of the same structure type but different oxygen content to understand the role of oxygen off-stoichiometry on the magnetic properties. 3. To measure electrical resistivity again to confirm the behavior and to analyze the electrical resistivity quantitatively using various models (thermally Activated and variable hopping range model). 4. To align the single-crystals using Laue camera. 5. To conduct magnetic measurements on the single-crystals Long-term plans: 1. If the grown single-crystals of the Brownmillerite phase show interesting magnetic behaviors, such as, signs of spin reorientations/multiple phase transitions etc. We will do dielectric measurements in collaboration with Dr. Sunil Nair

to look for possible multi-ferroicity in the compound. 2. One can also try to look at the Mossbauer spectroscopy on these compounds which can be done at Inter University Consortium of Department of Atomic Energy at Indore.

Bibliography

1. Dong, F., et al., La-doped $BaFeO_{3-\delta}$ perovskite as a cobalt-free oxygen reduction electrode for solid oxide fuel cells with oxygen-ion conducting electrolyte. *Journal of Materials Chemistry J. Mater. Chem.*, **2012.** 22(30): p. 15071-15079.

2. Dong, F., et al., $BaNb_{0.05}Fe_{0.95}O_{3-\delta}$as a new oxygen reduction electrocatalyst for intermediate temperature solid oxide fuel cells. *Journal of Materials Chemistry A J. Mater. Chem. A,* **2013**. 1(34): p. 9781-9791.

3. Itagaki, Y., et al., O_3 and NO_2 sensing properties of $SmFe_{1-x}Co_xO_3$ perovskite oxides. Sensors and Actuators B*: Chemical*, **2007**. 122(1): p. 315-320.

4. Jiang, S.P., et al., Electrical conductivity and performance of doped $LaCrO_3$ perovskite oxides for solid oxide fuel cells. *Journal of Power Sources*, **2008**. 176(1): p. 82-89.

5. Kusnezoff, M., FUEL CELLS " SOLID OXIDE FUEL CELLS | Membranes Encyclopedia of Electrochemical Power Sources, J.r. Garche, Editor. *Elsevier*: Amsterdam.**,2009**, p. 34-50.

6. Lucchini, E. and O. Sbaizero, High-temperature conductivity of the hexagonal form of $BaFeO_{3-x}$. *Journal of Materials Science Letters*, **1989**. 8(5 DO - 10.1007/BF00720286): p. 527-529 .

7. Singhal, S.C., Zirconia Electrolyte-based Solid Oxide Fuel Cells Encyclopedia of Materials: Science and Technology (Second Edition), K.H.J.r. Buschow, et al., Editors.*Elsevier: Oxford.* **2001**, p. 9898-9902.

8. Rakshit, S.K., et al., Thermodynamic properties of ternary oxides in the system $BaFeO_3$ using solid-state electrochemical cells with oxide and fluoride ion conducting electrolytes. *Journal of Solid State Chemistry*, **2004**. 177(4-5): p. 1146-1156.

9. Penwell, W.D. and J.B. Giorgi, Conductivity of cerium doped $BaFeO_{3-x}$ and applications for the detection of oxygen. Sensors and Actuators B*: Chemical*, **2014**. 191(0): p. 171-177.

10. Mengmeng Sun, Y.J., Fangfei Li, Maosheng Xia, Bing Xue and Darui Liu, Structure, Dye Degradation Activity and Stability of Oxygen Defective $BaFeO_{3-x}$. *Materials Transactions*, **2010**. Vol.51(No.11): p. 1981-1989.

11. Matsuno, J., et al., Different routes to charge disproportionation in perovskite-type Fe oxides. *Physical Review B*, **2002**. 66(19): p. 193103.

12. Rembelski, D., et al., Characterization and Comparison of Different Cathode Materials for SC-SOFC: LSM, BSCF, SSC, and LSCF. *Fuel Cells*, **2012**. 12(2): p. 256-264.

13. Kuo, J.H., H.U. Anderson, and D.M. Sparlin, Oxidation-reduction behavior of undoped and Sr-doped $LaMnO_3$: Defect structure, electrical conductivity, and thermoelectric power. *Journal of Solid State Chemistry*, **1990**. 87(1): p. 55-63.

14. Fergus, J.W., Perovskite oxides for semiconductor-based gas sensors. Sensors and Actuators B*: Chemical*, **2007**. 123(2): p. 1169-1179.

15. Moseley, P.T. and D.E. Williams, Gas sensors based on oxides of early transition metals. *Polyhedron*, **1989**. 8(13-14): p. 1615-1618.

16. Huang, S., et al., Bismuth-Based Pervoskite as a High-Performance Cathode for Intermediate-Temperature Solid-Oxide Fuel Cells. *ChemElectroChem*, **2014**. 1(3): p. 554-558.

17. Wang, H., et al., A Cobalt-Free Oxygen-Permeable Membrane Based on the Perovskite-Type Oxide $Ba_{0.5}Sr_{0.5}Zn_{0.2}Fe_{0.8}O_{3-x}$. *Advanced Materials*, **2005**. 17(14): p. 1785-1788.

18. Mori, S., Phase Transformation in Barium Orthoferrate, $BaFeO_{3-x}$. *Journal of the American Ceramic Society*, **1966**. 49(11): p. 600-605.

19. Mori, S., Magnetic Properties of Several Phases of Barium Orthoferrate, $BaFeO_x$. *Journal of the Physical Society of Japan J. Phys. Soc. Jpn.*, **1970**. 28(1): p. 44-50.

20. Ufaso, M.W.L., Prediction of the Cr ystal Str uctures of P erovskit es Using the Software Program SPuDS. **2001**.

21. Galakhov, V.R., et al., Valence Band Structure and X-ray Spectra of Oxygen-Deficient Ferrites $SrFeO_x$. *The Journal of Physical Chemistry C J. Phys. Chem. C*, **2010**. 114(11): p. 5154-5159.

22. Hayashi, N., et al., $BaFeO_3$: A Ferromagnetic Iron Oxide. *Angewandte Chemie International Edition*, **2011**. 50(52): p. 12547-12550.

23. Hook, H.J.V., Oxygen Stoichiometry in the Compound $BaFeO_{3-x}$. *The Journal of Physical Chemistry J. Phys. Chem.*, **1964**. 68(12): p. 3786-3789.

24. Iwahara, H., Ionic Conduction in Perovskite-Type Compounds, in Perovskite Oxide for Solid Oxide Fuel Cells, Ishihara, Editor,*Springer* US . **2009**. p. 45-63.

25. Kantiyong, L., Magnetism and mechanical properties of Barium ferrite-Natural Rubber composites. **2009.**

26. Chakraverty, S., et al., $BaFeO_3$ cubic single crystalline thin film: A ferromagnetic insulator doi:http://dx.doi.org/10.1063/1.4824210. *Applied Physics Letters*, **2013**. 103(14).

27. Ichida, T., et al., Mössbauer Study of Some Barium Orthoferrates. *Bulletin of the Institute for Chemical Research, Kyoto University*, **28-Jan-1974**. 51(5): p. 295.

28. MacChesney, J.B., et al., Oxygen Stoichiometry in the Barium Ferrates; Its Effect on Magnetization and Resistivity doi:http://dx.doi.org/10.1063/1.1726393. *The Journal of Chemical Physics*, **1965**. 43(9): p. 3317-3322.

29. K. J. Choi, Enhancement of Ferroelectricity in Strained BaTiO3 Thin Films, *Science* **5 November 2004**: 306 (5698), p.1005-1009.

30. W. Knafo,Ferromagnetism and lattice distortions in the perovskite YTiO3,*PHYSICAL REVIEW B79*, **2009,**054431.

31. Alexander Tkach,Fundamentals and Applications of $SrTiO_3$ and $KTaO_3$ based materials, Department of Physics of Science Faculty, IFIMUP, University of Porto, Portugal

32. Alistairr. Lennie,Cation ordering in $MgTi_2O_5$(karrooite): Probing temperature dependent effects with neutrons, *American Mineralogist*, **2007**, Volume 92, pages 1165-1180

33. B. V. Beznosikov, Perovskite-Like Crystals of the Ruddlesden–Popper Series,*Crystallography Reports*, , **2000**,Vol. 45, No. 5 .

34. S. Lambert,Modulated Distribution of Differently Ordered Tetrahedral Chains in the Brownmillerite Structure,*Chem. Mater.*, **2002**, 14 (4), pp 1818–1826

35. Hans D'Hondt,Tetrahedral Chain Order in the $Sr_2Fe_2O_5$ Brownmillerite,*Chem. Mater.*, **2008**, 20 (22), pp 7188–7194

36. Koushik Karmakar,Crystal Growth of the Nonmagnetic Zn^{2+} and Magnetic Co^{2+} Doped Quasi-One-Dimensional Spin Chain Compound $SrCuO_2$ Using the Traveling Solvent Floating Zone Method, *Cryst. Growth Des.*, **2014**, 14 (3), pp 1184–1192

37. K. A. Müller and H. Burkard ,$SrTiO_3$: An intrinsic quantum paraelectric below 4 K ,*Phys. Rev. B 19,*Published **1 April 1979** , *3593* .

38. Kunihito Koumoto,Oxide Thermoelectric Materials: *A Nanostructuring Approach,Annual Review of Materials Research* ,Volume publication date **August 2010,** *Vol. 40, 363-394.*

39. C. N. R. Rao,Multiferroic and Magnetoelectric Oxides: The Emerging Scenario,dx.doi.org/10.1021/ | *J. Phys. Chem. Lett.* ***2012****, 3, 2237−2246.*

40. N.L. Ross,High-pressure structural behavior of $GdAlO_3$ and $GdFeO_3$ perovskites, *Journal of Solid State Chemistry* , **October 2004**,*Volume 177, Issue 10*,Pages 3768–3775.

41. J .D. Lee,Concise Inorganic Chemistry 5th Edition.

42. G.H. Jonker,Ferromagnetic compounds of manganese with perovskite structure, *Physica,*, **March 1950**,*Volume 16, Issue 3,* Pages 337–349.

43. http://www.gotoknow.org/posts/564905.

44. Nancy L. Ross,Compressibility of brownmillerite ($Ca_2Fe_2O_5$): effect of vacancies on the elastic properties of perovskites,*Physics of the Earth and Planetary Interiors*,Volume 129, Issues 1–2, **1 January 2002**, Volume 129, Issues 1–2, Pages 145–151.

45. Sandra E. Dann,Reactions and Characterization of Solids,Publisher: Wiley-Rsc Publication Date: 2002.

46. Graham King ,Cation ordering in perovskites,*J. Mater. Chem.*, **2010**, 20, 5785-5796.,

47. Jung-Hoon Lee at al.,Spin-Canting-Induced Improper Ferroelectricity and Spontaneous Magnetization Reversal in $SmFeO_3$, Phys. Rev. Lett. 107, 117201 (2011),

48. Manekar et al.,First-order transition from antiferromagnetism to ferromagnetism in Ce(Fe0.96Al0.04)2,Phys. Rev B., **2001**, 64,104416.